Synconvergent ductile flow in variable-strength continental crust: Numerical models with application to the western Grenville orogen

R. A. Jamieson,[1] C. Beaumont,[2] M. H. Nguyen,[1,2] and N. G. Culshaw[1]

Received 11 August 2006; revised 30 March 2007; accepted 13 June 2007; published 25 September 2007.

[1] We present results from numerical models for a convergent orogen with laterally variable lower crustal strength, representing a simplified orogenic system in which a strong craton, flanked by progressively weaker terranes, collides with another continent. With progressive convergence, crustal thickening, and thermal relaxation, lower crust becomes decoupled from upper and middle crust, forming a ductile orogenic infrastructure beneath a stronger superstructure. Collision with strong external crust results in uplift and expulsion of ductile nappes from the orogenic core, creating allochthonous terranes overlying a lower crustal indentor. The extent of transport and exhumation of lower crustal nappes over the indentor reflects the amount of convergence and the erosion rate. The western Grenville orogen displays across-strike variations in age, tectonic history, and protolith association, suggesting a systematic variation in precollision crustal strength. The Laurentian craton, margin, and accreted terranes were variably reworked at synorogenic depths of 25–35 km during the Ottawan orogeny. Deformation propagated from younger monocyclic rocks in the southeast into older polycyclic rocks flanking the craton on the northwest. A comparison between numerical model results and crustal-scale cross sections from the Georgian Bay and Montreal–Val d'Or transects shows close correspondence between crustal structure and model geometry. This indicates that the models produce geologically realistic results and provides a context for interpreting the tectonic evolution of the western Grenville orogen. Contrasts between the results of homogeneous channel flow models and the present ductile nappe models suggest that the effects of different styles of ductile flow can be distinguished in the geologic record. **Citation:** Jamieson, R. A., C. Beaumont, M. H. Nguyen, and N. G. Culshaw (2007), Synconvergent ductile flow in variable-strength continental crust: Numerical models with application to the western Grenville orogen, *Tectonics*, *26*, TC5005, doi:10.1029/2006TC002036.

1. Introduction

[2] Although the effects of lower crustal ductile flow are well documented in many deeply eroded orogenic belts [e.g., *Bridgwater et al.*, 1974; *Myers*, 1978; *Davidson et al.*, 1994; *Northrup*, 1996; *Culshaw et al.*, 1997; *Williams and Hanmer*, 2006], a full explanation of the processes controlling this flow has remained elusive. Recently, the hypothesis that the geology and tectonics of the Himalayan-Tibetan system can be explained by midcrustal channel flow [e.g., *Bird*, 1991; *Westaway*, 1995; *Grujic et al.*, 1996; *Clark and Royden*, 2000; *Beaumont et al.*, 2001, 2004; *Jamieson et al.*, 2004; *Hodges*, 2006] has led to speculation about its possible role in other orogenic belts [e.g., *Husson and Sempere*, 2003; *St-Onge et al.*, 2006; *Godin et al.*, 2006; *Carr and Simony*, 2006; *Hatcher and Merschat*, 2006]. Do all large, hot orogens undergo some form of channel flow during their evolution, or is the postulated Himalayan channel flow a special case? In particular, does the style of lower crustal flow in accretionary orogens, constructed from contrasting crustal terranes, differ from that displayed by Himalayan-style orogens, constructed from laterally extensive passive continental margins?

[3] *Beaumont et al.* [2006] describe a range of flow modes in numerical models of large, hot, convergent orogens, with different styles of ductile flow related to different initial configurations of crustal strength. Here we present model results for a convergent orogen with laterally variable lower crustal strength. The initial conditions represent a simplified orogenic system in which a strong craton, flanked by progressively weaker (e.g., more juvenile) crustal-scale terranes, collides with another continent. With progressive convergence, crustal thickening, and thermal relaxation, lower crust becomes decoupled from upper and middle crust, forming a ductile orogenic infrastructure beneath a stronger superstructure [*Culshaw et al.*, 2006]. The model is used to investigate the effect of lateral strength variations on the thermal-mechanical evolution of large hot orogens, and demonstrates contrasting styles of upper and lower crustal deformation accompanying progressive convergence.

[4] The geological applicability of the model is tested against observations from the Grenville Province, the deeply eroded remnant of a large convergent orogen formed at the southeastern margin of Laurentia at circa 1200–1000 Ma [e.g., *Davidson*, 1984, 1995; *Rivers et al.*, 1989; *Carr et al.*, 2000; *Tollo et al.*, 2004; *Rivers et al.*, 2006]. Systematic across-strike variations in age, tectonic history, and inferred strength, developed during ~500 Ma of active continental margin tectonics, suggest that it is a suitable test case for the model style proposed here. In addition, widespread exposure

[1]Department of Earth Sciences, Dalhousie University, Halifax, Nova Scotia, Canada.
[2]Department of Oceanography, Dalhousie University, Halifax, Nova Scotia, Canada.

0278-7407/07/2006TC002036

of upper amphibolite to granulite facies gneisses and migmatites recording peak metamorphic conditions of $T \geq 750^{\circ}$C and $P \geq 10$ kb offers the opportunity to compare predicted styles of midcrustal flow with regional-scale observations from a natural laboratory. Model results are compatible with the crustal-scale geometry and thermal-tectonic evolution of the western part of the Canadian Grenville orogen, and provide an internally consistent framework for interpreting its first-order tectonic features. A detailed comparison between model results and a full range of structural, metamorphic, and geochronologic data from the orogen will be presented elsewhere.

2. Model Design and Initial Conditions

[5] The GO series uses a two-dimensional (2-D) finite element, thermal-mechanical numerical model [*Fullsack*, 1995] to compute the evolution of a model orogen subject to velocity boundary conditions applied at the sides and base of the model domain (Figure 1). Details of model design and formulation are presented elsewhere [e.g., *Fullsack*, 1995; *Beaumont et al.*, 2006]. A rationale for specific parameter choices and discussion of sensitivity to key factors is presented in the auxiliary material (see also appendix of *Beaumont et al.* [2006] and http://geodynamics.oceanography.dal.ca).[1] In order to focus on the physics of orogenic evolution, we choose the simplest model design that is compatible with the problem at hand, rather than attempting to simulate a particular natural example for which starting conditions may be poorly known. Previous models with laterally uniform material properties, e.g., representing broad passive continental margins, evolve to produce midcrustal channel flows [e.g., *Beaumont et al.*, 2001, 2004; *Jamieson et al.*, 2004, model HT1]. One goal of the present study is to determine whether or not similar flows develop in models with different initial crustal configurations. The GO series of models was designed to investigate the response to convergence of thick lower crust with laterally variable strength, e.g., as inherited from previous accretionary tectonic episodes [see also *Beaumont et al.*, 2006, model LHO-3; *Culshaw et al.*, 2006, model 1]. This factor was specifically excluded from Himalayan-Tibetan-style (HT) models, in which thin lower crust is subducted and plays no role in orogenic evolution [*Beaumont et al.*, 2004, 2006; *Jamieson et al.*, 2004]. Model parameters and important equations are listed in Table 1, and initial conditions are shown in Figure 1.

[6] The GO series models use a viscous-plastic rheology. In the plastic regime, variations in mechanical strength are controlled by the internal angle of friction, ϕ_{eff}, which includes the effects of variable pore fluid pressure (Table 1). Flow is viscous when the flow stress is less than the plastic yield stress for the local ambient conditions. In the ductile regime, effective viscosities (η_{eff}) are determined by power law creep flow laws (Table 1) with the values of B^*, n, and Q based on two well-constrained reference materials (wet Black Hills quartzite (WQ) [*Gleason and Tullis*, 1995] and dry Maryland diabase (DMD) [*Mackwell et al.*, 1998]). Model materials are made stronger or weaker by linearly scaling B^* values up or down. The scaled viscosities can be interpreted in terms of variable bulk composition or water content, or can be viewed simply as synthetic model rheologies [*Beaumont et al.*, 2006]. Since contrasting flow behaviors of different model materials mainly reflect viscosity contrasts, this scaling means that, for the same ambient conditions, the viscosity contrast is given by the scaling factor.

[7] The models include upper, middle, and lower crustal layers with contrasting material properties (Figure 1). Model properties are symmetric about the center (Figure 1a) except that the proflank of the orogen is mildly denuded by slope-dependent erosion [e.g., *Beaumont et al.*, 2004, 2006], whereas the retroside is not (details in section 3.2). The upper and middle crustal layers are laterally uniform. The upper crust (initially 0–10 km) has $B^* = B^*(WQ)$ and $\phi_{\text{eff}} = 5^{\circ}$, which can be interpreted to represent quartz-rich upper crustal rocks with high pore fluid pressure. The middle crust (initially 10–20 km) uses $B^* = B^*(WQ)x5$ and $\phi_{\text{eff}} = 15^{\circ}$, which can be interpreted as quartzo-feldspathic (meta)sedimentary or granitic rocks with hydrostatic fluid pressure. Heat production in the upper and middle crust (0–20 km) is uniform, with $A_1 = 2.0\ \mu\text{W m}^{-3}$, representing dominantly (meta)sedimentary and/or felsic igneous rocks.

[8] The rheology of the proside lower crust includes an outboard strong region (B^*(DMD), block F), flanked by five systematically weaker lower crustal blocks (Figure 1a), each initially 250 km wide and 15 km thick. From the edge of block F to the center of the model, the rheologies of these blocks are successively reduced from the reference B^*(DMD) value by factors of 4, as follows: B^*(DMD)/4 (block E), B^*(DMD)/8 (block D), B^*(DMD)/12 (block C), B^*(DMD)/16 (block B), and B^*(DMD)/20 (block A). The resulting effective viscosities are equivalent to dry diabase or refractory mafic granulite (B^*(DMD)), through intermediate granulite (B^*(DMD)/12), to quartz-rich and/or partially hydrated granulite or amphibolite (B^*(DMD)/20). All lower crustal materials are assigned a nominal value of $\phi_{\text{eff}} = 15^{\circ}$, which plays no role because deformation is entirely in the ductile regime. Heat production in the lower crust (20–35 km) is uniform, with $A_2 = 0.75\ \mu\text{W m}^{-3}$, representing partially depleted mafic or intermediate granulite.

[9] A central strong lower crustal block (block G; 250 km wide; B^*(DMD)) separates the proside and retroside of the system. This block serves as a marker and ensures that both promargin and retromargin are bounded by equivalently strong crust. The presence or absence of a strong central block influences deformation only within ~50 km of the S point (compare model LHO-3 of *Beaumont et al.* [2006]). Sensitivity experiments demonstrate that the strength of the opposing margin, including the presence or absence of block G, plays no role in the creation and expulsion of the ductile nappes that are the focus of the present study.

[10] An important component of Himalayan-style channel flow models is a linear decrease in effective viscosity from the flow law value at $T = 700^{\circ}$C to 10^{19} Pa s at $T \geq$

[1] Auxiliary materials are available in the HTML. doi:10.1029/2006TC002036.

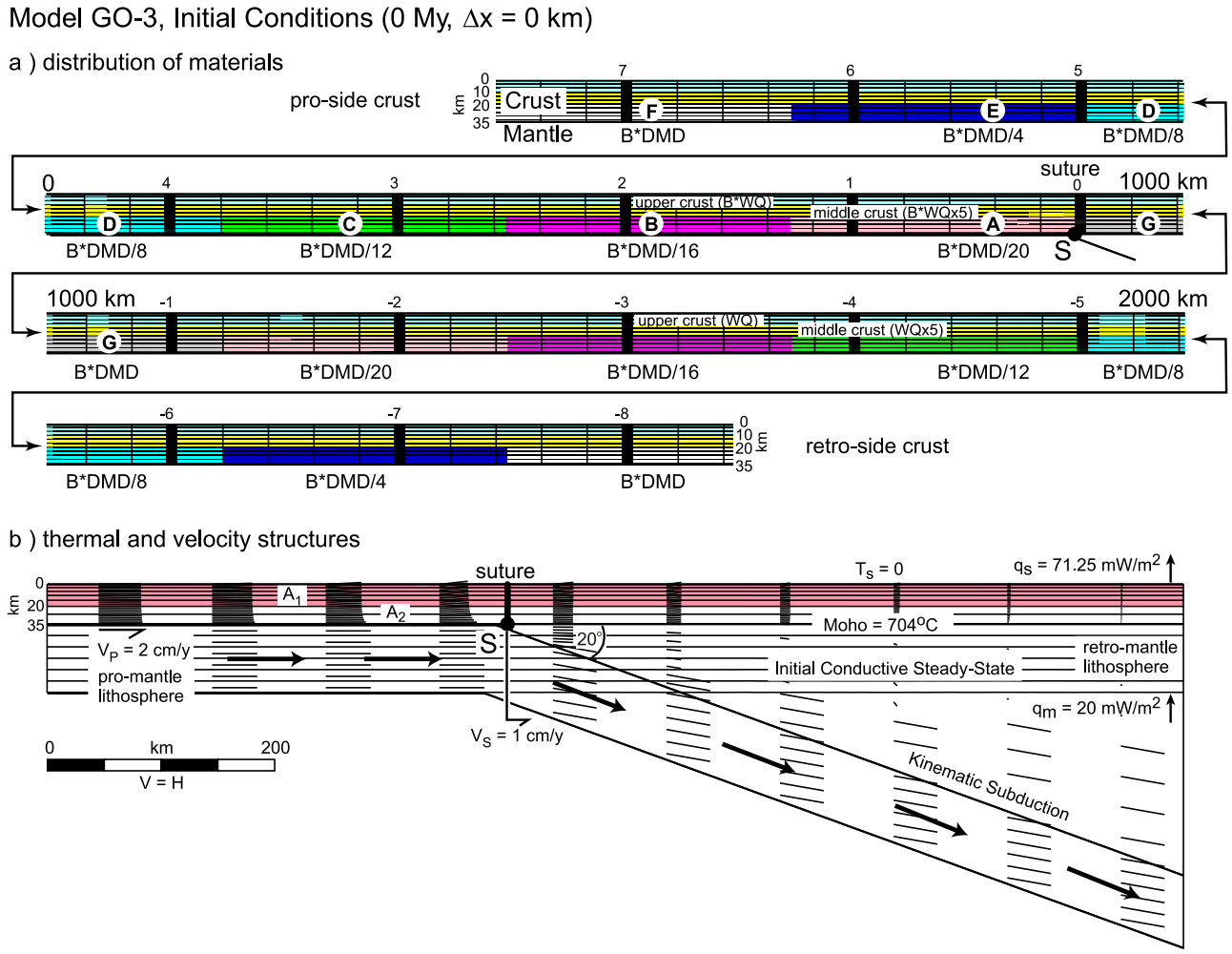

Figure 1. Initial conditions, GO-model series (0 My = 0 Ma(emt) = millions of years elapsed model time). (a) Initial distribution of materials and passive marker grid. Upper (B^*(WQ)) and middle crust (B^*(WQx5)) have laterally uniform properties, whereas lower crustal strength is decreased systematically from B^*(DMD) to B^*(DMD/20) to approximate a continental margin consisting of a craton flanked by progressively weaker reworked and/or accreted terranes (for further details, see text and Table 1). Width of model domain is 2000 km. Blocks labeled A–G are tracked during model evolution (Figures 2 and 3). Deformation is displayed using a passive marker grid in which initial vertical markers are spaced at 40 km and horizontal markers at 5 km, with heavy vertical markers, initially at 200 km intervals, numbered outward from the suture (0). (b) Initial thermal structure. The model includes two laterally uniform heat-producing crustal layers (A_1, A_2); the combination of basal mantle heat flux, q_m = 20 mW m^{-2}, and crustal heat production leads to an initial surface heat flux, q_s = 71.25 mW m^{-2}, and T_{Moho} = 704°C. The model is started in conductive steady state. Convergence velocity, V_P = 2 cm a^{-1}, and subduction zone advance, V_S = 1 cm a^{-1}; mantle lithosphere detaches at point S, with kinematic subduction at 20°. For a full explanation of model design, including velocity reference frame and comparisons between kinematic and dynamic subduction models, see *Beaumont et al.* [2006, http://geodynamics.oceanography.dal.ca] and the auxiliary material.

750°C [*Beaumont et al.*, 2001, 2004]. This "melt weakening" approximates the reduction in bulk viscosity caused by a small amount of in situ partial melt (≤7% [e.g., *Rosenberg and Handy*, 2005]). In GO series models, melt weakening is incorporated into the upper and middle crustal layers (those based on the $B^*(WQ)$ flow law), which are interpreted to include a significant proportion of (meta)sedimentary and/or juvenile felsic igneous rocks. The lower crust, interpreted to represent variably depleted mafic to intermediate granulite and/or igneous rocks, is not affected by melt weakening at temperatures reached in the lower orogenic crust. Variable ductile flow behavior in the lower crust is therefore entirely attributable to the strength variations imposed by scaling $B^*(DMD)$. Relative to Himalayan channel flow models, in

Table 1. Parameters Used in Models[a]

Parameter	Meaning	Value(s)
	Mechanical Parameters	
ρ_{crust}	crustal density	2700 kg m^{-3}
ρ_{mantle}	mantle density	3300 kg m^{-3}
D	flexural rigidity in isostasy model	10^{22} Nm
	crustal thickness	35 km
	lower crustal thickness	15 km
	width of Eulerian model domain	2000 km
$(J_2')^{1/2} = P\sin\,\phi_{\text{eff}} + C$	Drucker-Prager yield criterion where ϕ_{eff} defined by $P\sin\,\phi_{\text{eff}} = (P - P_f)\sin\,\phi$ for assumed values of P_f	
ϕ_{eff} (0–10 km)	effective internal angle of friction (upper crust)	5°
ϕ_{eff} (10–35 km)	effective internal angle of friction (midcrust and lower crust)	15°
C	cohesion	10 MPa
P	dynamical pressure (mean stress)	Pa
P_f	pore fluid pressure	Pa
J_2'	second invariant of the deviatoric stress tensor	Pa^2
$\eta_{eff}(^v = B^*(\dot{I}_2')^{(1-n)/2n}\exp[Q/nRT_K]$	general equation for effective viscosity	
I_2'	second invariant of strain rate tensor	s^{-2}
R	gas constant	8.314 J (mol °K)$^{-1}$
T_K	absolute temperature	°K
B^*, n, Q as below		
WQ (0–10 km)	wet Black Hills quartzite flow law [after *Gleason and Tullis*, 1995]	n = 4.0, B^* = 2.92 × 10^6 Pa $s^{1/4}$, Q = 223 kJ mol^{-1}
WQ × 5 (10–20 km)	modified wet Black Hills quartzite flow law (as above except scaled by 5)	$B^* = B^*$ (WQ) × 5
DMD (20–35 km)	dry Maryland diabase flow law [after *Mackwell et al.*, 1998]	n = 4.7, B^* = 1.91 × 10^5 Pa $s^{1/4.7}$, Q = 485 kJ mol^{-1}
DMD flow law scaled by weakening factor, w, DWD/w, where w = 4, 8, 12, 16, 20		
DMD/w	modified dry Maryland diabase flow law	$B^* = B^*$ (DMD)/w
melt weakening	linear reduction in effective viscosity over T range 700–750°C for WQ and WQ × 5 only	η_{700} = flow law value, $\eta_{750} = 10^{19}$ Pa s
	Basal Velocity Boundary Conditions	
V_P	left-side (convergence) velocity	2 cm a^{-1}
V_R	right-side velocity	0 cm a^{-1}
V_S	S point velocity	1 cm a^{-1}
	Thermal Parameters	
$\rho C_p\partial T/\partial t + \underline{v}\cdot\nabla T = K\nabla^2 T + A$	heat balance equation	
C_p	specific heat	750 m^2 K^{-1} s^{-2}
K	thermal conductivity	2.00 W (m°K)$^{-1}$
κ	thermal diffusivity ($\kappa = K/\rho Cp$, where $\rho Cp = 2 \times 10^6$)	1.0 × 10^{-6} m^2 s^{-1}
T_s	surface temperature	0°C
T_a	temperature at lithosphere/asthenosphere boundary	1350°C
q_m	basal mantle heat flux	20 m W m^{-2}
q_s	initial surface heat flux	71.25 mW m^{-2}
A_1 (0–20 km)	upper crustal heat production	2.0 × 10^{-6} W m^{-3}
A_2 (20–35 km)	lower crustal heat production	0.75 × 10^{-6} W m^{-3}
	Surface Denudation (*Proside Only*, Figure 3)	
slope × $f(t)$ × $g(x)$	denudation rate	
slope	local surface slope (measured from finite element mesh)	
$f(t)$	time function (specifies how denudation rate (m a^{-1}) varies with time when $g(x)$ and slope = 1)	
$g(x)$	spatial function (specifies how denudation rate varies with position x); $g(x)$ = 0 = arid and $g(x)$ = 1 = wet	
$f(t)$	GO-1, 0	$t > 0$ (i.e., constant)
	GO-2, 0.0133 m a^{-1}	
	GO-3, 0.0266 m a^{-1}	
	GO-4, 0.0399 m a^{-1}	
$g(x)$	1.0	$0 < x \leq 500$ km
$g(x)$	varies linearly 1.0 → 0.0	$500 < x < 550$ km
$g(x)$	0.0	$x \geq 550$ km

[a]See Figures 1, 2, and 3. Details of model design, choice of parameters, and implementation are given by *Fullsack* [1995], *Beaumont et al.* [2004], *Beaumont et al.* [2006], and the auxiliary material.

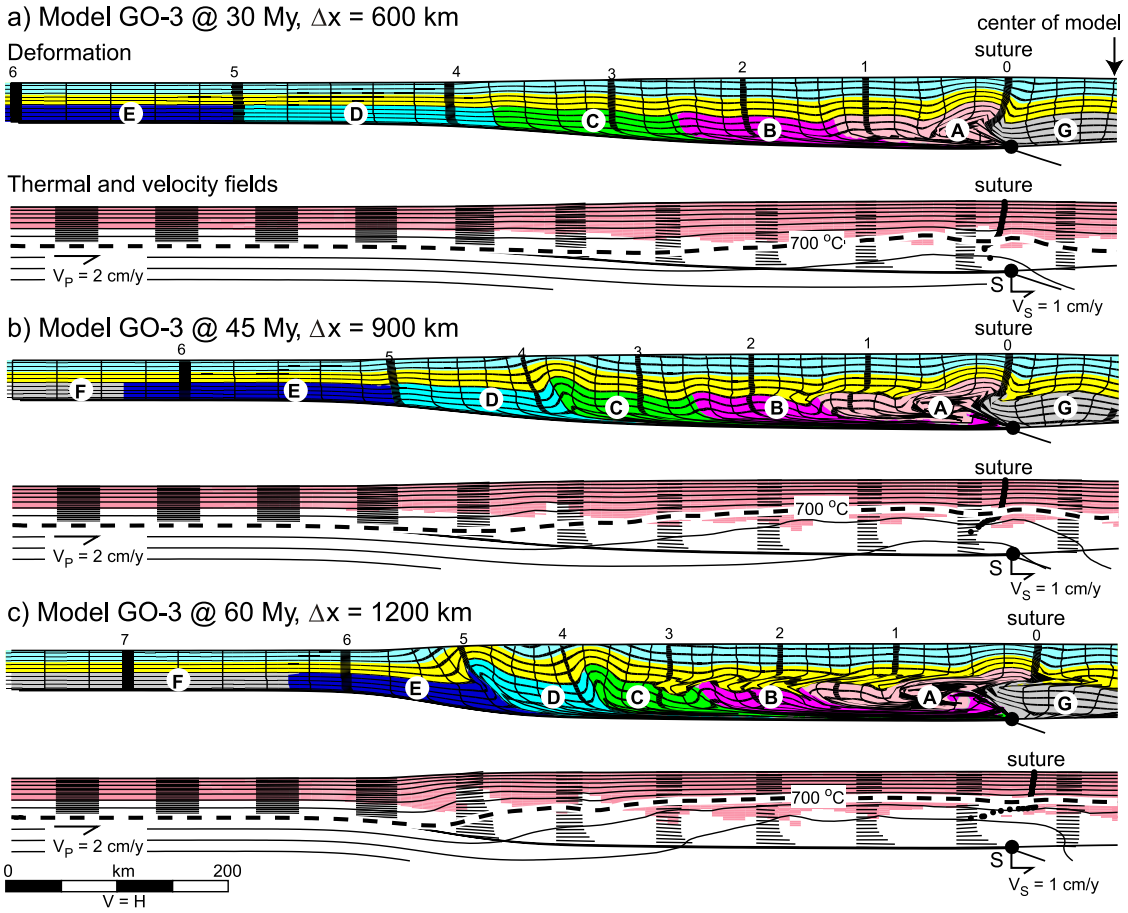

Figure 2. Progressive evolution of model GO-3, illustrating main features of GO series as a whole. Only proside model results are shown, corresponding to 0–1000 km in Figure 1a, retroside (no erosion) resembles the proside of model GO-1 (Figure 3a). (top) Deformation of material blocks and passive marker grid (Δx, total convergence); (bottom) distribution of heat-producing layers (shaded, A_1; white, A_2), isotherms (100°C intervals), and velocity field. Material shading as in Figure 1a; 700°C isotherm is melt-weakening threshold (upper and middle crust only). (a) Model GO-3 at 30 Ma(emt) (My = Ma(emt)) after the onset of convergence: upright structures throughout crust. (b) Model GO-3 at 45 Ma(emt), asymmetric structures developing in lower crustal blocks A, B, C. (c) Model GO-3 at 60 Ma(emt). Block E has reached outer edge of orogen, blocks A, B, and lower middle crust shows initial stages of lateral ductile flow. (d) Model GO-3 at 75 Ma(emt). Strong external block F has just reached flank of orogen, with significant lateral flow in blocks A, B, and lower middle crust. (e) Model GO-3 at 90 Ma(emt). Block F forms strong indentor, underthrusting weaker internal materials; blocks E and D have been transported over the lower crustal ramp at the leading edge of block F. (f) Model GO-3 at 105 Ma(emt). Block F has penetrated ~400 km beneath the orogen, and leading edges of blocks E, D, and C have become detached from their roots and transported and partially exhumed above lower crustal indentor. For further discussion, see text. (An animation of this model can be viewed at: http://geodynamics.oceanography.dal.ca.)

which lower crust is subducted, a much smaller proportion of GO series model crust is susceptible to melt weakening because the upper middle crust is thinner (20 versus 25 km), and the thicker lower crust (15 versus 10 km), which is not affected by melt weakening, accumulates in the orogen rather than being subducted.

[11] The initial structure of the GO series models is shown in Figure 1. The initial crustal structure is symmetrical about the center of the model (Figure 1a), except that the S point is located at the proward edge of strong central block G. Initially vertical passive markers at 200 km intervals are numbered outward from 0 (model suture) to 9. For the thermal parameter values used (Table 1), and a basal heat flux, q_m = 20 mW m^{-2}, the initial surface heat flux (q_s) is 71.25 mW m^{-2} and the Moho temperature (T_{Moho}) is 704°C (Figure 1b). Velocity and deformation are calculated dynamically in the crust, whereas the mantle velocity field is prescribed kinematically. In these models,

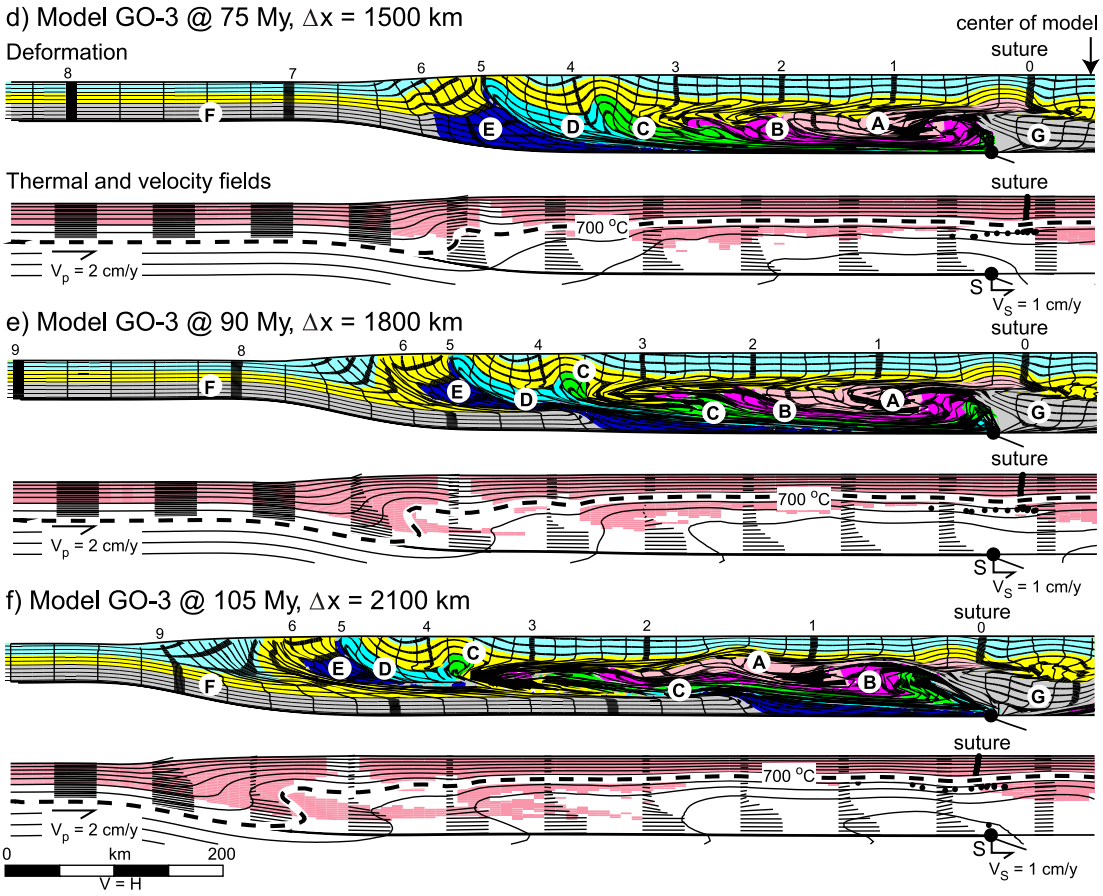

Figure 2. (continued)

the prolithosphere converges on the stationary retrolithosphere at $V_P = 2$ cm a^{-1}, and the S point advances at $V_S = 1$ cm a^{-1} (Figure 1b). The subducted mantle lithosphere descends at constant dip with constant kinematically specified velocity. Although these velocities are imposed on the model, they are consistent with the results of dynamic subduction model experiments that display subduction zone advance [e.g., *Beaumont et al.*, 2006]. Work in progress on dynamic subduction models with variable-strength lower crust demonstrates that subduction style does not affect lower crustal deformation in GO-type models.

3. Model Results

[12] The GO series consists of four models (GO-1 to GO-4) that differ only in the intensity of erosion applied to the proside of the system. We first present results from the proside of model GO-3 (moderate erosion), which demonstrates the characteristic features of the GO series as a whole. The erosion model and the effects of variable erosion rate are discussed in section 3.2. Figure 2 shows deformation (Figure 2, top) and thermal and velocity fields (Figure 2, bottom) for a series of time steps from 30 to 105 Ma(emt). Model times are quoted in millions of years elapsed model time (Ma(emt)); here we reserve the notation Ma (millions of years before present) for ages of geological features and events.

3.1. Evolution of Model GO-3 During Progressive Convergence

[13] Figures 2a–2c show model evolution during the early stages of crustal thickening, thermal relaxation, and ductile flow (30–60 Ma(emt); $\Delta x = 600$–1200 km). For the first 30 Ma(emt), the entire model crust progressively shortens and thickens almost homogeneously (Figure 2a). A basal shear zone develops between the lower crustal blocks and the underlying mantle lithosphere, which does not deform. Initially, while the thickened crust is still cool, isotherms are stretched vertically, but thermal relaxation after ~20 Ma(emt) leads to significant heating in the orogenic core, with $T \geq 800$°C in the lowermost crust by 30 Ma(emt) (Figure 2a).

[14] Figure 2b, which shows the model at 45 Ma(emt) ($\Delta x = 900$ km), illustrates the diachronous deformation of the lower crustal blocks. As each block enters the model orogen it first thickens, with initially vertical markers remaining nearly vertical except in the basal shear zone. The outer edge of each internal block is thrust over the adjacent, stronger block as incoming blocks are drawn into the basal shear zone, producing asymmetrical folds at block

margins. As convergence proceeds, these folds become progressively tighter and more asymmetrical (compare blocks A and C), eventually forming recumbent fold nappes. Except in the vicinity of the suture, the vergence of these lower crustal structures is proward, toward the foreland.

[15] At 45 Ma(emt), the weakest lower crustal block (A) at the center of the model has become detached from the base of the crust and thrust over adjacent stronger blocks (B and G), forming a doubly vergent structure that persists through subsequent model evolution. Asymmetrical structures have begun to develop in the adjacent outboard blocks (B, C). The upper and middle crustal layers have thickened substantially, and a decoupling zone has begun to develop between the middle and lower crust above blocks A and B (vicinity of marker 1). The decoupling zone is restricted to the midcrustal layer where $T \geq 700^{\circ}$C (Figure 2b, bottom) and which is therefore susceptible to melt weakening. A plateau has developed at the model surface above the weak midcrustal region. This process continues through 60 Ma(emt) (Figure 2c), when block E has reached the outer edge of the orogen. By this time, internal lower crustal blocks (A, B) have begun to form fold nappes that are subsequently transported, along with immediately overlying weak midcrust, over adjacent outboard blocks.

[16] Figures 2d–2f show the evolution of lower crustal deformation from 75 Ma(emt) to 105 Ma(emt) (Δx = 1500–2100 km) and illustrate the response of the model orogen to the arrival of strong external crust. At 75 Ma(emt) (Figure 2d), lower crustal block F (B*(DMD)) is just about to enter the deforming region. Adjacent block E has thickened substantially but has not developed the recumbent nappes characteristic of internal blocks A to D. This marks a transition in the deformation style, whereby strong outboard lower crust begins to resist the highly ductile flow characteristic of weaker materials in the orogenic core. At this time the lower crust is dominated by shallow dipping ductile structures verging toward the foreland, whereas upper and middle crust remain dominated by upright structures. The decoupling zone in melt-weakened midcrust extends across most of the center of the model (between markers 1 and 3). Velocity profiles and deformation of vertical markers suggest that material within the decoupling zone is flowing toward the orogenic flank at a faster rate than materials above and below, forming a thin (<5 km), incipient midcrustal channel [e.g., *Beaumont et al.*, 2001]. Moderate erosion at the plateau flank leads to partial exhumation of lower crust, with block D within 5 km of the surface by 75 Ma(emt). Thickening of block E and partial exhumation of block D are reflected in the asymmetric thermal structure near the orogenic flank (Figure 2d, bottom).

[17] By 90 Ma(emt) (Figure 2e), the arrival of lower crustal block F has produced a change in tectonic style beneath the edge of the plateau. This block resists deformation and underthrusts previously deformed lower crustal material, forming a strong indentor that is progressively transported into the model orogen. The leading edge of the indentor acts as a lower crustal ramp. At 90 Ma(emt), blocks E and D have been transported up this ramp, forming coherent thrust sheets that are in the process of being detached from their roots and exhumed by the combination of underthrusting and surface erosion. The leading edge of block C has reached the ramp at the edge of the indentor. As it overrides the strong ramp, the shallow dipping nappe at the "nose" of this block is rotated, uplifted, and eventually detached (Figure 2f). Inboard of the indentor, the model orogen consists of shallow dipping thrust sheets, separated from upright upper crustal structures by a decoupling zone displaying incipient channel flow. Some middle crustal material has been drawn down into the lower crustal ductile flow zone, notably in the region between blocks C and B.

[18] At the end of the model evolution (105 Ma(emt), Δx = 2100 km), block F has penetrated more than 400 km beneath the orogen (Figure 2f). The detached nose of block C has been transported more than 250 km over the ramp, and is separated from the rest of block C by a region of hot, strongly deformed middle crust infolded with material derived from blocks A and B. Total displacement of the block C klippe therefore represents the combined effects of stretching and dismemberment of the original material and lateral transport of the detached block within the midcrustal flow zone. Between the indentor and the suture, the lower orogenic crust consists of highly attenuated, shallow to moderately dipping sheets. As block F is transported into the orogen, these are progressively thrust over the lower crustal ramp, forming a stack of ductile thrust sheets dipping toward the orogenic core. The upper and middle crust at the flank of the orogen have been variably thickened, folded, and partially eroded in response to exhumation of lower crustal blocks, in contrast to the upright upper crustal structures in the orogenic core. Beneath the plateau, hot middle crust ($T \geq 700^{\circ}$C) has been thinned by ductile flow and locally incorporated into the lower midcrustal flow zone so that it partly underlies detached lower crustal nappes. Isotherms in the orogenic core are nearly horizontal, but are steep to overturned where hot lower crustal nappes have been transported over the cooler lower crustal indentor.

3.2. Effect of Erosion

[19] Syntectonic erosion has a demonstrable effect on orogenic architecture [e.g., *Koons*, 1989; *Willett*, 1999; *Zeitler et al.*, 2001]. In the present models, erosion rate is determined by an imposed spatial function ($g(x)$), which controls where erosion operates in the model, an imposed intensity function ($f(t)$), which controls the efficiency of erosion with time and incorporates the combined effects of factors such as precipitation, relief, discharge, and bedrock properties, and a surface slope function, which is determined by the model [*Beaumont et al.*, 2004, 2006]. In all the GO series models, erosion is restricted to the proside of the model plateau (Table 1), representing the asymmetric distribution of orographic rainfall as displayed by modern orogens with large plateaus. The effect of erosion intensity on tectonic evolution was tested by systematically varying the erosion function from 0 to 3 between models (Table 1). Model design is otherwise identical. Here we compare the results of model GO-3 (moderate erosion) with models GO-1 (no erosion), GO-2 (weak erosion), and GO-4 (strong erosion). Equivalent maximum rates of erosion at 90 Ma(emt)

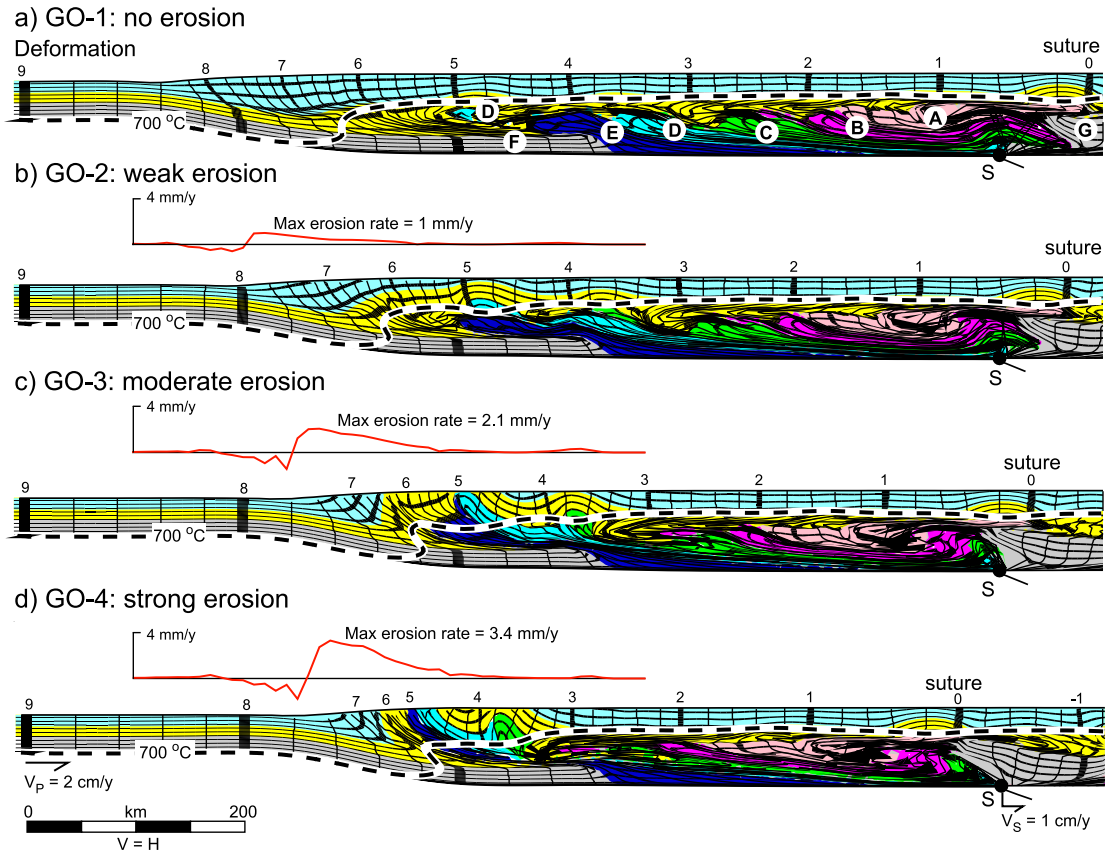

Figure 3. Effect of variable erosion rate on tectonic evolution, models GO-1 to GO-4, shown at 90 Ma(emt) (My = Ma(emt)). Shading and material properties are as in Figure 1; for clarity, the lower crustal blocks are only labeled in Figure 3a. Region shown corresponds to 0–1000 km (Figure 1a). Erosion rate plots show slope-dependent variation in erosion rate across the orogenic flank at this time; erosion rate of 0 is beyond the plotted range; erosion rate <0 indicates subsidence and deposition in the foreland basin. (a) Model GO-1, no erosion (erosion function 0; erosion rate 0 mm a^{-1} and is not shown). b) Model GO-2, weak erosion (erosion function = 1; maximum erosion rate = 1 mm a^{-1}); an additional result from this model at 82.5 Ma(emt) is shown in Figure 7b. (c) Model GO-3, moderate erosion (erosion function 2; maximum erosion rate 2.1 mm a^{-1}); additional results shown in Figure 2. (d) Model GO-4, strong erosion (erosion function 3, maximum erosion rate 3.4 mm a^{-1}). Model properties are otherwise identical. Note, in particular, the contrast in orogen width, transport distance of allochthons over the lower crustal indentor (compare positions of blocks E, D, and C and vertical marker 3), and the extent of exhumation between models GO-1 and GO-2 (wider orogen, low degrees of allochthoneity and exhumation) and models GO-3 and GO-4 (narrow orogen, high degrees of allochthoneity and exhumation). For further discussion, see text.

range from 0 mm a^{-1} in GO-1 to ~4 mm a^{-1} in GO-4 (Table 1 and Figure 3).

[20] Figure 3 shows proside results from the four models at 90 Ma(emt), arranged in order of increasing erosion intensity. The retrosides of the models are not eroded and resemble proside results from model GO-1 (no erosion; Figure 3a) (see also model 1 of *Culshaw et al.* [2006]). In low-erosion models GO-1 and GO-2, the model orogen is significantly wider than GO-3, because little or no mass is removed from the system. Although the orogens are wider, there is less transport of lower crustal nappes over the indentor in the low erosion rate models (compare positions of blocks D and E with marker 3). Erosion rate therefore affects the degree of allochthoneity (transport distance from precollision position) and amount of nappe stacking and flattening, with the extent of extrusion of material from beneath the plateau correlating with the amount of material eroded from the orogen flanks. Exhumation of lower crustal nappes in low erosion rate models is also suppressed relative to model GO-3. Instead, as lower crustal nappes are underthrust by the strong indentor, they are transported laterally ~150 km at midcrustal levels (Figures 3a and 3b). This flow mode resembles channel "tunneling" in laterally homogeneous Himalayan-style models [*Beaumont et al.*, 2004], and can be interpreted as a form of heterogeneous channel flow in which detached fragments of lower crustal

nappes are transported within the melt-weakened decoupling zone (''lumpy channel'' [e.g., *Jamieson et al.*, 2005]).

[21] In models GO-3 and GO-4, with moderate to high erosion rates, the model orogen is not as wide as it is in low erosion rate models, because more mass is removed from the system. In these models, lower crustal blocks D and E are exhumed during and after transport over the strong indentor, with block D reaching the model surface by 90 Ma(emt) in both cases. The resulting midcrustal structure near the orogenic front consists of moderately dipping, relatively thick thrust sheets of lower crustal material, rather than the flat-lying, highly attenuated nappes characteristic of the low erosion rate models. Since the position and the style of the model orogenic front are determined within the model rather than being predefined, these results suggest that erosion rate exerts a strong influence on equivalent structures in natural systems. Midcrustal structure beneath the plateau regions is similar in all four models, and erosion has relatively little effect on the position of the 700°C isotherm, although near-surface isotherms (not shown) are condensed in high erosion rate models.

[22] In summary, syntectonic erosion rate has a significant effect on the style and amount of exhumation of lower crustal blocks above the strong indentor, with a marked contrast in the behavior of model GO-2 (weak erosion) and that of model GO-3 (moderate erosion). In particular, the degree of syntectonic exhumation of lower crustal nappes and the tectonic style of the orogenic front differ significantly between low and high erosion rate end-members. These contrasts should be detectable in nature, although the distinction between no versus weak erosion, or moderate versus strong erosion, is unlikely to be evident in deeply eroded natural orogens.

3.3. Tectonic Interpretation of Model Results

[23] The contrast between upright upper crustal structures and shallow dipping lower crustal structures is characteristic of this model style [e.g., *Culshaw et al.*, 2006], and results from the contrasting rheological behavior of upper, middle, and lower crustal materials under the prevailing thermal conditions. The results can be interpreted in terms of diachronous three-phase evolution of orogenic superstructure and infrastructure [e.g., *Beaumont et al.*, 2006; *Culshaw et al.*, 2006]. During phase 1, the crust progressively shortens and thickens by nearly uniform contraction. Phase 2 involves thermal relaxation of thickened crust to produce hot, variably ductile middle and lower crust (infrastructure) and relatively cool, strong, frictional-plastic upper crust (superstructure). Phase 3 involves tectonic activation of ductile flow in response to underthrusting of strong lower crust, which forces weaker middle and lower crust into large-scale, gently inclined, ductile nappes that root at the Moho. Each vertical crustal column that enters the model orogen is affected by the same set of processes, but at sequentially later times, with the specific response depending on lower crustal strength. For example, block A has experienced phase 1 contraction and early phase 2 thermal relaxation by 30 Ma(emt) (Figure 2a), before blocks D and E have even entered the orogen. Equivalent structures on each side of the model orogen thus get younger from the core toward the flanks, and phase 1 upper crustal structures are older than phase 3 lower crustal structures that underlie them. The time taken to thicken, heat, and weaken each crustal column to the threshold of ductile flow is referred to as the incubation time [*Beaumont et al.*, 2006; *Culshaw et al.*, 2006]. For the parameters used in the GO series, the minimum incubation time is ~20 Ma(emt), but lateral transport of lower crustal nappes (phase 3) is not activated until strong lower crust is advected into the orogen. Phase 3 flow begins after 50 Ma(emt) in the hot, weak orogenic core, and by 75 Ma(emt) affects the whole orogen, as strong external lower crust (blocks E, F) is thrust beneath weaker internal blocks.

[24] During progressive convergence, lower crustal blocks are deformed into increasingly asymmetric structures, with the innermost, weakest block (A) thrust over stronger adjacent blocks on both sides. As convergence continues, weaker internal nappes are progressively expelled into the midcrust and transported over the indentor, where they may be exhumed by erosion. The resulting orogen (Figure 2f) consists of ductile infrastructure (lower and midcrustal nappes) partly overlying the underthrust indentor and decoupled from the stronger superstructure by a subhorizontal ductile high-strain zone that displays incipient channel flow beneath the plateau. As noted above, the extent of transport and exhumation of lower crustal nappes during phase 3 flow is affected by erosion rate, and total displacement includes transport of detached fragments in flowing midcrust as well as bulk transport of coherent thrust sheets.

[25] The equivalent natural orogen would display increasing strain from the strong (cratonic) foreland toward the orogenic core, where ductile nappes formed from more distal, weaker crustal blocks, would display substantial (>100 km) foreland directed transport. Where preserved, middle crust would display shallow, highly ductile, migmatitic fabrics, and upper crust would display upright structures with little evidence of synconvergent ductile deformation or high-grade metamorphism. Ages of lower crustal metamorphism and deformation would young toward the foreland, with upper crust preserving older ages than subjacent lower crustal rocks.

4. Application to the Western Grenville Orogen

[26] The Grenville orogen represents the exposed midcrustal levels of a large collisional orogenic system developed on the southeastern margin of Laurentia at circa 1200–1000 Ma [e.g., *Davidson*, 1984, 1995; *Rivers et al.*, 1989, 2006]. Prior to the onset of Grenvillian convergence, the region was occupied by a long-lived (>500 Ma), southward building, continental magmatic arc and back-arc system [e.g., *Dickin and McNutt*, 1991; *Rivers*, 1997; *Rivers and Corrigan*, 2000; *Slagstad et al.*, 2004a; *Tollo et al.*, 2004]. The present architecture of the orogen formed largely during the Ottawan and Rigolet phases of the Grenvillian orogeny (circa 1090–

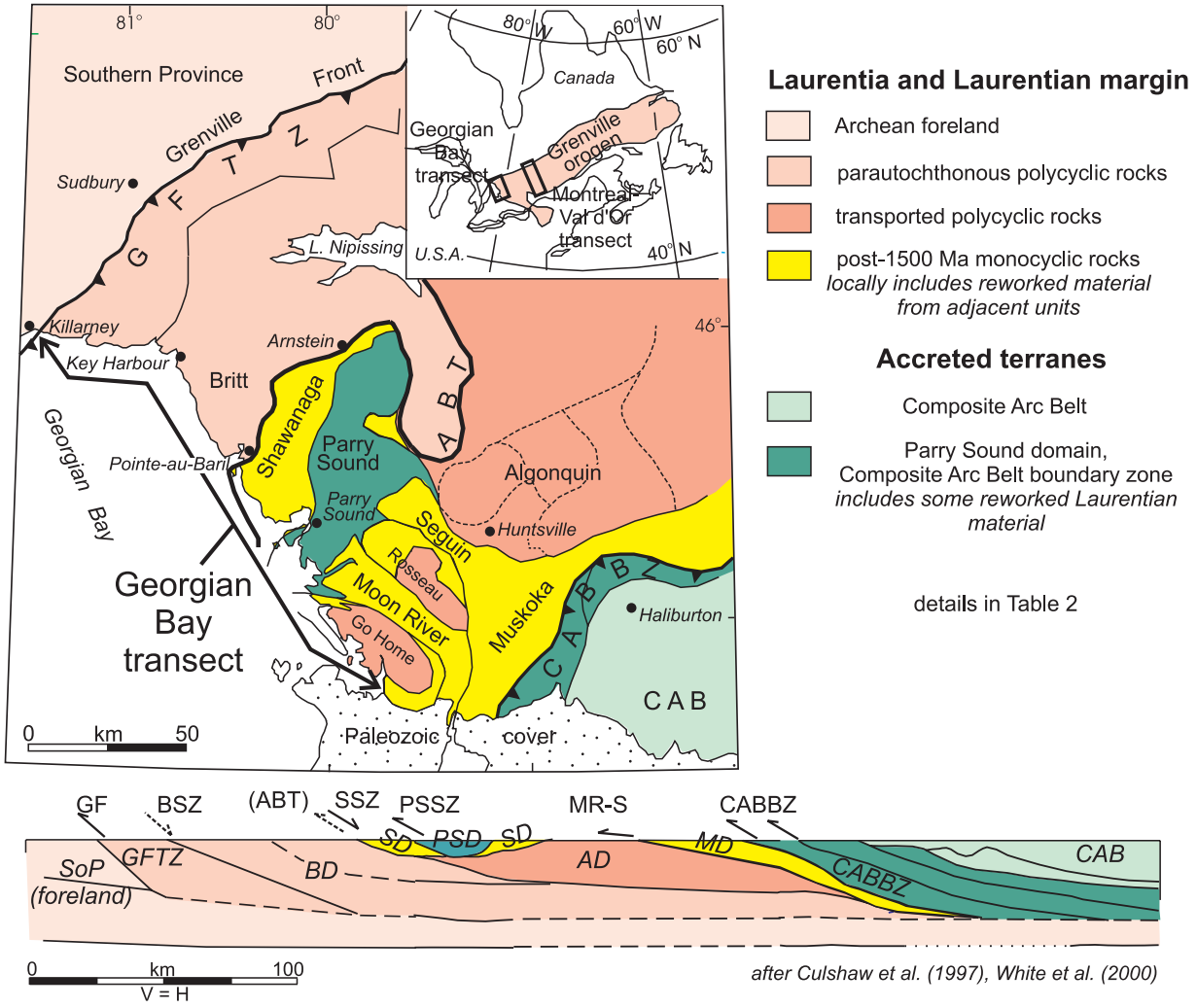

Figure 4. Regional geology of the western Grenville orogen in Ontario [after *Culshaw et al.*, 1997; *Ketchum and Davidson*, 2000], showing the location of the Georgian Bay transect. Inset shows location of transects discussed in this paper within the Grenville orogen as a whole. Crustal-scale cross section is constructed from geological and seismic data by *Culshaw et al.* [1997], with modifications after *White et al.* [2000]. For a summary of geological and structural features, abbreviations, and references, see Table 2.

990 Ma) with some important features inherited from earlier accretion (circa 1280–1120 Ma).

[27] At the western end of the orogen, crustal-scale cross sections and comprehensive regional tectonic syntheses [e.g., *Culshaw et al.*, 1997; *Carr et al.*, 2000; *Martignole et al.*, 2000], constructed by integrating geological data with geophysical data collected during the Lithoprobe program, allow convenient comparison of observations with model results. This part of the orogen displays a transition from Archean crust in the foreland, to Paleo-Mesoproterozoic crust affected by both pre-Grenvillian and Grenvillian high-grade metamorphism (polycyclic), to Mesoproterozoic crust displaying only Grenvillian metamorphism (monocyclic). The crustal-scale geology is broadly consistent with decreasing lower crustal strength from northwest (foreland) to southeast (orogenic core). The predominance of northwest–southeast trending lineations and a relative scarcity of oblique structures suggest that Ottawan convergence was approximately orthogonal, with transport from southeast to northwest. On this basis, we infer that observations from the western part of the orogen can be used to test the geological applicability of the 2-D GO series models. Here we compare data from the Georgian Bay transect [*Culshaw et al.*, 1997] with results from model GO-3, and data from the Montreal–Val d'Or transect [*Martignole et al.*, 2000] with results from model GO-2.

4.1. Georgian Bay Transect

[28] *Culshaw et al.* [1997] presented a crustal-scale cross section (Figure 4) based on a well-exposed geological transect along the shores of Georgian Bay, Ontario, integrated with Lithoprobe seismic data [*White et al.*, 1994, 2000]. The cross section has been interpreted to reflect

Table 2. Summary of Important Geological Units and Structures Along the Georgian Bay Transect[a]

Name and Abbreviation	Description and Significance
	Laurentia and Laurentian Margin
Southern Province (SoP)	Neoarchean margin of Superior Province; some Paleoproterozoic and Mesoproterozoic igneous rocks; not affected by Grenvillian ductile deformation or metamorphism; orogenic foreland [*Wynne-Edwards*, 1972; *Card*, 1990; *Davidson*, 1992; *Bethune*, 1997]
Grenville Front Tectonic Zone (GFTZ)	polycyclic Paleoproterozoic to Mesoproterozoic gneisses; parautochthonous (can be linked to foreland);cut by Sudbury diabase (circa 1235 Ma); late Grenvillian (circa 1000 Ma, "Rigolet") amphibolite facies metamorphism; belt of crustal-scale, thrust sense, ductile shear; northern flank of Grenville orogen; proximal Laurentian crust during Ottawan convergence [*Wynne-Edwards*, 1972; *Haggart et al.*, 1993; *Krogh*, 1994; *Bethune*, 1997]
Britt domain (BD)	polycyclic, parautochthonous, Paleoproterozoic to Mesoproterozoic migmatitic orthogneiss, including circa 1450 Ma granulite; cut by Sudbury diabase; Ottawan (circa 1060–1035 Ma) upper amphibolite facies metamorphism and deformation; proximal Laurentian crust [*Corrigan et al.*, 1994; *Ketchum et al.*, 1994; *Culshaw et al.*, 1997; *Ketchum and Davidson*, 2000].
Shawanaga domain (SD)	here includes upper Go Home and upper Rosseau domains (south of PSD); monocyclic migmatitic paragneisses and orthogneisses; cut by Algonquin gabbros (circa 1170 Ma); Ottawan (circa 1085–1050 Ma) upper amphibolite facies metamorphism with local granulite, relict high-pressure rocks; Mesoproterozoic (circa 1500–1350 Ma) continental magmatic arc–back arc; Laurentian midcrust during Ottawan convergence [*Culshaw et al.*, 1994, 1997; *Culshaw and Dostal*, 1997; *Ketchum et al.*, 1998; *Ketchum and Davidson*, 2000; *Wodicka et al.*, 2000; *Slagstad et al.*, 2004a, 2004b]
Algonquin domain (AD)	here includes lower Go Home and lower Rosseau domains; polycyclic orthogneiss with minor paragneiss; cut by Algonquin gabbros; Ottawan (circa 1090–1050 Ma) upper amphibolite to granulite facies metamorphism; local relict high-pressure metamorphism; transported distal Laurentian lower crust [*Davidson*, 1995; *Culshaw et al.*, 1997; *Nadeau and van Breemen*, 1998; *Ketchum and Davidson*, 2000]
Muskoka domain (MD)	migmatitic orthogneiss derived from Mesoproterozoic (1500–1350 Ma) continental magmatic arc rocks (granodiorite with minor granite, diorite, gabbro); affected by Ottawan (circa 1080–1060 Ma) high-grade metamorphism and partial melting; forms substantial component of Moon River–Seguin lobe structures; Laurentian midcrust [*Timmermann et al.*, 1997; *Slagstad et al.*, 2004a, 2004b, 2005].
	Accreted Terranes
Parry Sound domain (PSD)	mafic to intermediate orthogneiss with minor paragneiss; protolith ages circa1400–1330 Ma; early Grenvillian (circa 1160 Ma, "Shawinigan") granulite facies metamorphism; variable Ottawan (circa 1090–1060 Ma) amphibolite facies retrogression and structural reworking; allochthonous fragment of accreted terrane [*van Breemen et al.*, 1986; *Davidson*, 1986b, 1995; *Wodicka et al.*, 1996, 2000; *Culshaw et al.*, 1997]
Composite Arc Belt (CAB)	formerly referred to as Central Metasedimentary Belt; oceanic and microcontinental terranes (protolith ages circa 1300–1230 Ma), pre-Grenvillian (circa 1290–1230 Ma) deformation and metamorphism ("Elzevir" stage) interpreted to represent offshore terrane assembly; limited Ottawan medium- to low-grade metamorphism and brittle deformation; interpreted as upper crustal superstructure during Ottawan deformation and metamorphism [*Easton*, 1992; *Corfu and Easton*, 1995, 1997; *Carr et al.*, 2000]
	Major Structures
Grenville Front (GF)	NW limit of Grenvillian deformation and metamorphism; brittle-ductile thrust faults bounding crustal-scale zone of ductile thrust sense shear (GFTZ), associated with rapid exhumation and cooling at circa 1000 Ma [*Wynne-Edwards*, 1972; *Davidson*, 1986a; *Krogh*, 1994]
Boundary shear zone (BSZ)	boundary between GFTZ and BD; moderately dipping ductile shear zone with oblique-normal kinematics; age poorly constrained, circa 1000–1030 Ma [*Jamieson et al.*, 1995]
Allochthon Boundary Thrust (ABT)	ABT represents cryptic thrust boundary between allochthonous Laurentian rocks with local relict HP assemblages (SD, AD) and parauthochthonous Laurentian crust (BD); reworked as

Table 2. (continued)

Name and Abbreviation	Description and Significance
Shawanaga Shear Zone (SSZ)	ductile normal sense SSZ (circa 1020 Ma) along Georgian Bay transect [*Rivers et al.*, 1989, 2002; *Culshaw et al.*, 1994; *Ketchum et al.*, 1998; *Ketchum and Davidson*, 2000]
Parry Sound Shear Zone (PSSZ)	granulite facies ductile thrust zone (circa 1160 Ma) separating interior PSD from basal PSD; transported within PSD during Ottawan convergence [*van Breemen et al.*, 1986; *Wodicka et al.*, 1996; *Culshaw et al.*, 1997]
Moon River–Seguin structures (MR-S)	NW trending, highly migmatitic, lobate synformal structures extending from MD toward PSD; include reworked MD and PSD lithologies; syn-Ottawan ductile flow (incipient channel?); Seguin lobe pre-1045 Ma [*Davidson*, 1984; *Culshaw et al.*, 1997; *Slagstad et al.*, 2005; *Krogh and Kwok*, 2005]
Composite Arc Belt boundary zone (CABBZ)	formerly referred to as Central Metasedimentary Belt boundary (thrust) zone; includes both reworked Laurentian gneisses and material derived from accreted terranes; Ottawan (circa 1080–1030 Ma) amphibolite facies metamorphism and ductile deformation; transition zone from ductile Laurentian infrastructure to CAB superstructure [*Carlson et al.*, 1990; *Hanmer and McEachern*, 1992; *Burr and Carr*, 1994; *Carr et al.*, 2000]

[a]See Figure 4.

progressive northwest directed transport of Laurentian crust and accreted terranes during the Ottawan and Rigolet orogenic phases (circa 1090–990 Ma [*Jamieson et al.*, 1992, 1995; *Culshaw et al.*, 1997; *Carr et al.*, 2000]). Geological units and structures are summarized in Table 2. From north to south the key features include (1) Neoarchean rocks of the foreland (Southern Province, SoP), inferred to extend beneath the northwestern flank of the orogen; (2) parautochthonous, polycyclic Laurentian orthogneisses (Grenville Front Tectonic Zone, GFTZ; Britt domain, BD) affected by both pre-Grenvillian and Grenvillian high-grade metamorphism; the GFTZ represents a late Grenvillian (circa 1020–990 Ma, Rigolet stage of *Rivers and Corrigan* [2000]) crustal-scale, thrust sense shear zone [e.g., *Green et al.*, 1988; *Haggart et al.*, 1993; *Krogh*, 1994] bounded on the north by the Grenville Front (GF) and on the south by the ductile, oblique-normal boundary shear zone (BSZ [*Jamieson et al.*, 1995]); (3) voluminous monocyclic orthogneisses and paragneisses derived from the products of circa 1500–1350 Ma continental arc magmatism (Shawanaga domain, SD; Muskoka domain, MD, and equivalents) [e.g., *Culshaw and Dostal*, 1997; *Slagstad et al.*, 2004a]; (4) polycyclic orthogneisses of the distal Laurentian margin (Algonquin domain, AD, and equivalents); Algonquin and Shawanaga domain rocks are separated from underlying rocks by the Allochthon Boundary Thrust (ABT, post-1090 Ma [*Rivers et al.*, 1989; *Ketchum and Davidson*, 2000]), which was later reactivated as the ductile normal-sense Shawanaga shear zone (SSZ, circa 1020 Ma [*Culshaw et al.*, 1994; *Ketchum et al.*, 1998]); (5) a highly allochthonous fragment of an accreted terrane (Parry Sound domain, PSD), separated from underlying Laurentian rocks by the pre-Ottawan, granulite facies, thrust sense Parry Sound Shear Zone (PSSZ, circa 1160 Ma [*van Breemen et al.*, 1986]); and (6) accreted juvenile (circa 1300–1230 Ma) oceanic and continental terranes (Composite Arc Belt, CAB), recording only minor Ottawan deformation and metamorphism, separated from Laurentian rocks to the northwest by a crustal-scale ductile thrust belt (Composite Arc Belt boundary zone, CABBZ) that includes both reworked Laurentian gneisses and high-grade equivalents of CAB lithologies [*Carr et al.*, 2000].

[29] Except for the foreland and CAB, the entire transect was affected by Grenvillian upper amphibolite to granulite facies metamorphism and ductile strain. Ages of peak metamorphism and deformation get progressively younger from southeast to northwest [*Jamieson et al.*, 1992; *Culshaw et al.*, 1997; *Wodicka et al.*, 2000]. In addition, PSD records early (circa 1160 Ma) granulite facies metamorphism and thrusting not present in adjacent and underlying rocks. On the basis of contrasts in protolith ages, time and grade of peak metamorphism, and structural and geophysical features, the PSD has been interpreted as an allochthonous klippe derived from accreted terranes further to the southeast [e.g., *Davidson*, 1984; *White et al.*, 1994; *Wodicka et al.*, 1996; *Culshaw et al.*, 1997]. At the southeastern end of the transect, CAB rocks were affected by deformation and medium- to low-grade metamorphism at circa 1280–1230 Ma (Elzevirian orogeny), interpreted to reflect offshore assembly prior to Grenvillian collision [*Carr et al.*, 2000]. Between the PSD and CAB, the thin, lobate, migmatitic Moon River and Seguin structures (MR-S), including reworked equivalents of PSD and MD lithologies [*Slagstad et al.*, 2004b, 2005; *Krogh and Kwok*, 2005], are interpreted to have formed during northwest directed ductile flow. The high metamorphic grade, predominance of shallow to moderately dipping structures, and abundant evidence for pervasive ductile flow and flattening strain led *Culshaw et al.* [1997] to conclude that most of the Georgian Bay transect region lay beneath an orogenic plateau during the Ottawan orogeny. In contrast, the limited effects of Ottawan metamorphism and deformation on the CAB suggest that it represented the orogenic superstructure during this time [*Culshaw et al.*, 2004].

[30] Figure 5 shows model GO-3 at 97.5 Ma(emt) compared with the Georgian Bay cross section. At this stage of model evolution, the lower crustal indentor has penetrated more than 300 km beneath the orogen (Figure 5b). Blocks E

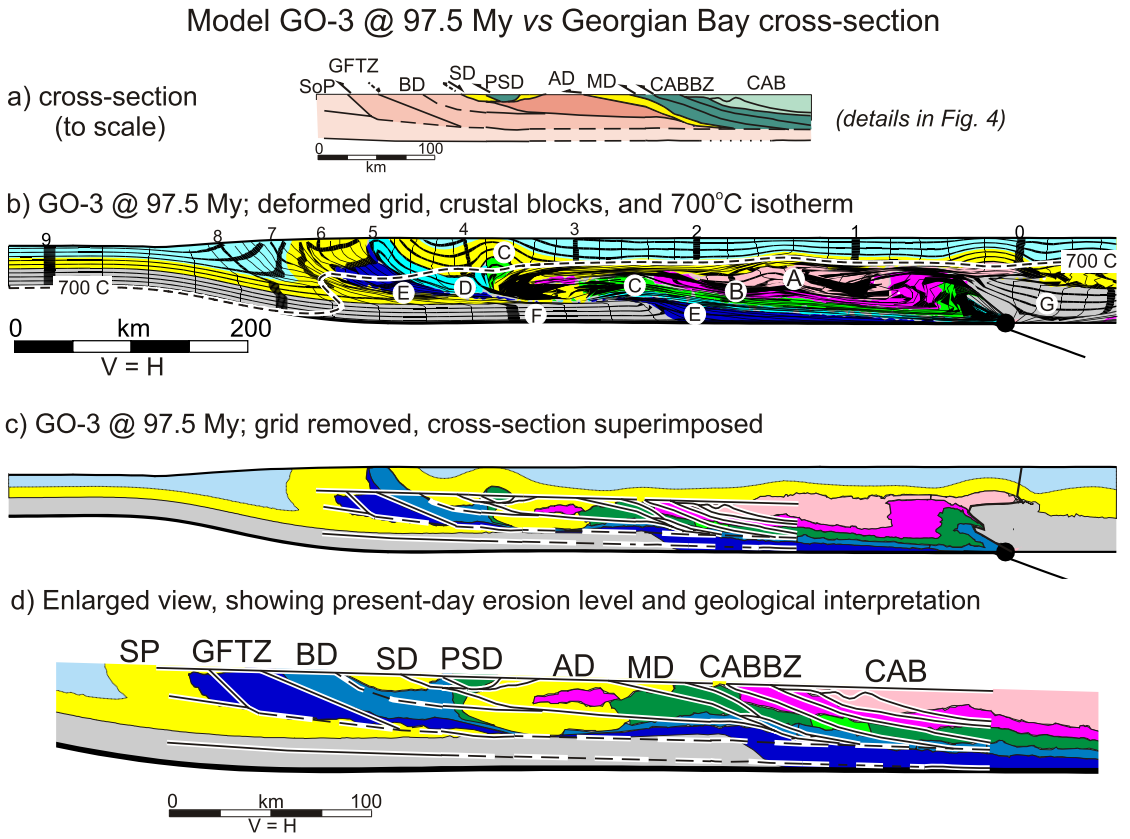

Figure 5. Model GO-3 compared with the Georgian Bay cross section. (a) Crustal-scale cross section (Figure 4) at same scale as model. (b) Model result at 97.5 Ma(emt) (My = Ma(emt), showing deformed crustal blocks, marker grid, and 700°C isotherm. Detached nappes (E, F, part of C) transported and partly exhumed over lower crustal indentor (F), weak middle crust incorporated into lower crustal flow zone between allochthonous crust and infrastructure in orogenic core. (c) Model result with marker grid removed for clarity, Georgian Bay cross section superimposed. (d) Enlarged view of Figure 5c, showing present-day erosion level and geological interpretation. PSD corresponds to detached "nose" of block C, parautochthon (GFTZ, BD) corresponds to allochthonous ductile thrust sheets D and E, and SD and MD correspond to melt-weakened middle crust, infrastructure consists of moderately dipping thrust sheets of all lower crustal blocks overlain by CAB superstructure. For further discussion, see text.

and F have been transported over the indentor and partly exhumed, forming large coherent thrust sheets with moderate dips. The detached nose of block C has been transported more than 100 km over the ramp and is separated from the rest of block C by a region of strongly deformed middle crust infolded with material from blocks A and B. Between the indentor and the suture, the orogenic infrastructure consists of a stack of ductile thrust sheets dipping toward the orogenic core. Beneath the plateau, upright upper crustal structures are preserved, and the underlying middle crustal layer has been thinned by ductile flow at $T \geq 700$°C and locally incorporated into the lower crustal ductile flow zone. Isotherms in the orogenic core are nearly horizontal (Figure 5b), but are steep to overturned where hot nappes have been transported over cooler incoming lower crust. Figure 5c shows a line drawing of the cross section superimposed on the 97.5 Ma(emt) model result. The model and cross section were aligned so that the Parry Sound domain (PSD) matches the position of the detached block C klippe, with the Moho at the base of the model. Aligned in this way, the GF lies near the outer edge of block E, the GFTZ-BD boundary matches the boundary between blocks E and D, and the CABBZ matches the position of the imbricate ductile thrust sheets from which the detached nappes have been derived (Figure 5d).

[31] Specific hallmarks of the Georgian Bay transect that fit model GO-3 are (1) seismic and other evidence of underthrusting by the strong Archean Superior craton; (2) highly allochthonous domains that have been detached and transported over the indenting Laurentian craton; (3) the crustal-scale ramp that provides evidence of the transport of lower crustal material over the leading edge of the indentor; (4) the final structural level occupied in the crust by the various transported domains which, when combined with evidence concerning their composition and older peak metamorphism, indicates that they were elevated from lower to midcrustal levels during Ottawan convergence, presumably by transport up and over the crustal ramp;

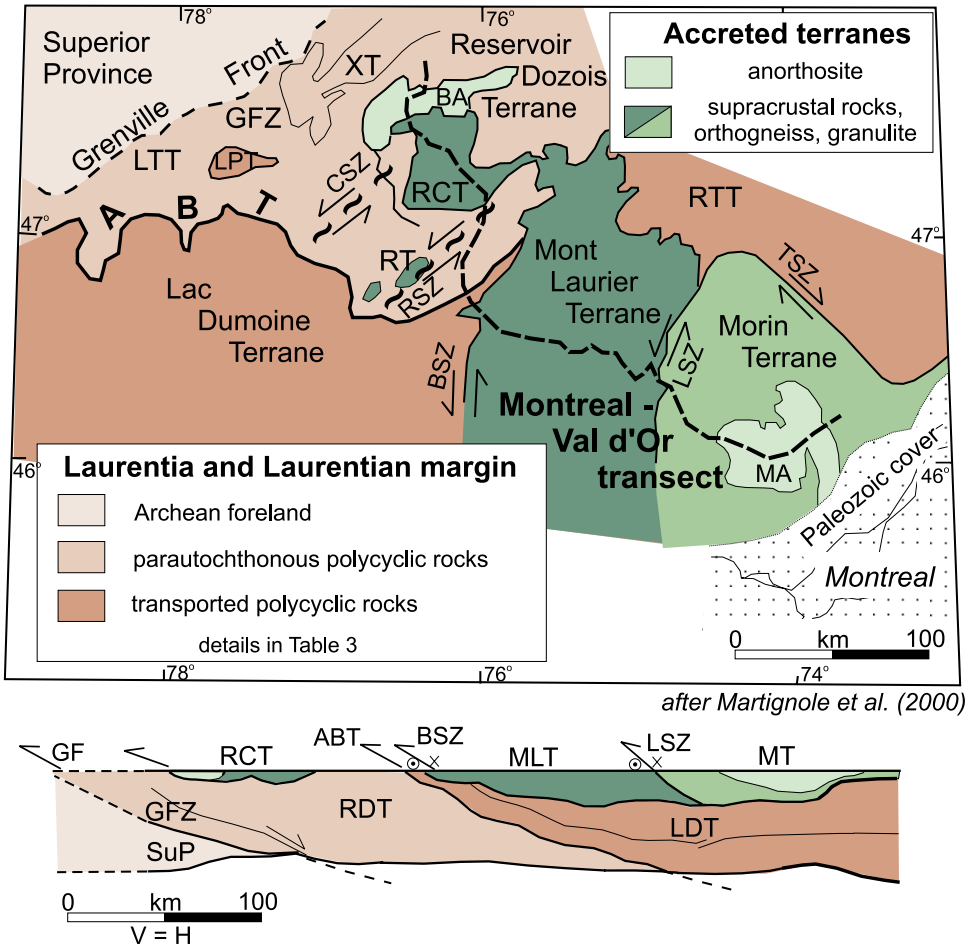

Figure 6. Regional geology of the western Grenville orogen in southwestern Quebec [after *Martignole et al.*, 2000], showing the location of the Montreal–Val d'Or transect (see also inset, Figure 4). Crustal-scale cross section constructed from geological and seismic data by *Martignole et al.* [2000]. For a summary of geological and structural features, abbreviations, and references, see Table 3.

(5) the "last in–first out" stacking order of lower crustal blocks, consistent with systematic stacking of weaker (monocyclic) over stronger (polycyclic) domains; and (6) the incorporation of melt-weakened middle crust into the lower crustal ductile flow zone, consistent with the distribution of highly migmatitic rocks (SD, MD) surrounding the PSD klippe. These hallmarks are achieved in GO-1 at 97.5 Ma(emt), after approximately 400 km of underthrusting by strong lower crust; work in progress shows that they are largely preserved during postconvergent ductile extension.

[32] The close correspondence between the geometry of the model and the geometry of the cross section strongly suggests that processes like those incorporated into model GO-3 are responsible for the crustal architecture of the Georgian Bay transect. Nevertheless, there are some discrepancies between the model and the cross section. In particular, the model predicts that detached nappes derived from accreted terranes (blocks A, B) should be present in the region that is entirely occupied by the Laurentian Algonquin domain (AD). Implications for both the model and the Georgian Bay transect are discussed in section 5.

4.2. Montreal–Val d'Or Transect

[33] *Martignole et al.* [2000] presented a crustal-scale cross section (Figure 6) based on a geological transect between Montreal and Val d'Or, Quebec, integrated with Lithoprobe seismic data. Although there are significant differences from the Georgian Bay transect, the dominant features along the cross section are also interpreted to have formed during progressive transport of Laurentian crust and accreted terranes from southeast to northwest during the Ottawan and Rigolet stages of orogeny [e.g., *Indares and Martignole*, 1990a, 1990b; *Childe et al.*, 1993; *Friedman and Martignole*, 1995]. Geological units and structures are summarized in Table 3. The key features, from north to south, include (1) Mesoarchean rocks of the foreland (Superior Province, SuP), inferred to extend beneath the northwestern flank of the orogen; (2) parautochthonous,

Table 3. Summary of Important Geological Units and Structures Along the Montreal–Val d'Or Transect[a]

Name and Abbreviation	Description and Significance
	Laurentia and Laurentian Margin
Superior Province (SuP)	Mesoarchean Superior Province; not affected by Grenvillian ductile deformation or metamorphism; orogenic foreland [*Indares and Martignole*, 1989; *Martignole et al.*, 2000]
Grenville Front Zone (GFZ)	here includes Lac Timiskaming (LTT) and X (XT) terranes; Archean to Paleoproterozoic amphibolite facies supracrustal rocks and orthogneisses (LTT); parautochthonous, locally gradational contacts with Archean foreland; includes polycyclic Neoarchean felsic to intermediate granulites with Proterozoic metamorphic overprint (XT); bounded on north by Grenville Front (GF) and grades into RDT to the south; short-lived HP event 995–1020 *Indares and Martignole*, 1989; *Childe et al.*, 1993; *Martignole and Reynolds*, 1997; *Martignole et al.*, 2000]
Reservoir Dozois Terrane (RDT)	polycyclic, parautochthonous, Archean to Paleoproterozoic migmatitic orthogneiss, cut by circa 1215 Ma coronitic metagabbro; Ottawan (circa 1060–1020 Ma) upper amphibolite faces metamorphism and deformation [*Indares and Dunning*, 1997; *Martignole et al.*, 2000]
Lac Dumoine Terrane (LDT)	here includes Lac Perche (LPT) and Reservoir Taureau (RTT) terranes; heterogeneous Paleoproterozoic to Mesoproterozoic orthogneiss and paragneiss with coronitic metagabbro; circa 1070 Ma Ottawan high-grade metamorphism, local relict high-pressure assemblages; separated from underlying parautochthonous rocks by Allochthon Boundary Thrust [*Indares and Dunning*, 1997; *Martignole et al.*, 2000; *Rivers et al.*, 2002]
	Accreted Terranes (*Frontenac-Adirondack Belt, FAB*)
Reservoir Cabonga Terrane (RCT)	here includes the highly deformed Bouchette anorthosite (BA); elsewhere dominantly metasedimentary gneisses; high-grade metamorphism 1160–1180 Ma, probable northern lobe of Mont Laurier Terrane; separated from underlying rocks by NW directed ductile thrusts [*Friedman and Martignole*, 1995]
Mont Laurier Terrane (MLT)	here includes Renzy Terrane (RT); Mesoproterozoic platformal metasediments with minor metaplutonic rocks (Frontenac equivalents); circa 1160–1190 Ma upper amphibolite to granulite facies metamorphism and anorthositic magmatism; lacks high-grade Ottawan overprint; separated from underlying rocks by pre-1080 Ma Baskatong Shear Zone (BSZ) [*Friedman and Martignole*, 1995; *Corriveau and van Breemen*, 2000; *Harris et al.*, 2001]
Morin Terrane (MT)	includes Morin anorthosite (MA; 1155 Ma) and related rocks intruded into granulite facies supracrustal rocks and orthogneiss (Adirondack equivalents); separated from MLT by Labelle Shear Zone (LSZ); extent of Ottawan overprint not clear [*Doig*, 1991; *Martignole*, 1995]
	Major Structures
Grenville Front (GF)	circa 1000 Ma crustal-scale thrust with superimposed normal faults cutting Moho [*Indares and Martignole*, 1989; *Childe et al.*, 1993; *Martignole and Calvert*, 1996]
Renzy and Cadgecrib shear zones (RSZ, CSZ)	circa 1000 Ma sinistral transcurrent shear zones [*Martignole and Friedman*, 1998; *Martignole et al.*, 2000]
Allochthon Boundary Thrust (ABT)	pre-1020 Ma thrust separating LDT and overlying rocks from underlying parautochthon [*Rivers et al.*, 1989, 2002; *Martignole et al.*, 2000]
Baskatong Shear Zone (BSZ)	includes Cabonga thrust; pre-1020 Ma sinistral shear zone, probably reactivated Ottawan or older (pre-1080 Ma) thrust; separates RCT and MLT from underlying parautochthon [*Friedman and Martignole*, 1995; *Martignole*, 1995]
Labelle and Taureau shear zones (LSZ, TSZ)	pre-1077 Ma sinistral (LSZ) and dextral (TSZ) shear zones separating MT from underlying rocks [*Martignole and Friedman*, 1998; *Martignole et al.*, 2000]

[a]See Figure 6.

polycyclic Laurentian orthogneisses (Grenville Front Zone, GFZ; Reservoir Dozois Terrnae, RDT; and associated terranes; Table 3) affected by both pre-Grenvillian and Grenvillian high-grade metamorphism [e.g., *Indares and Martignole*, 1989, 1990a]; (3) polycyclic paragneisses and orthogneisses of the distal Laurentian margin (Lac Dumoine Terrane, LDT, and equivalents); LDT rocks are separated from underlying rocks by the Allochthon Boundary Thrust (ABT [*Rivers et al.*, 1989, 2002; *Martignole et al.*, 2000]); and (4) allochthonous accreted terranes (including Reservoir Cabonga, RCT, Mont Laurier, MLT, and Morin, MT, terranes), including anorthosite bodies and related rocks (Bouchette, BA, and Morin, MA, anorthosites), separated from underlying Laurentian rocks by the Baskatong Shear Zone (BSZ) and equivalent structures [e.g., *Harris et al.*, 2001; *Martignole et al.*, 2000].

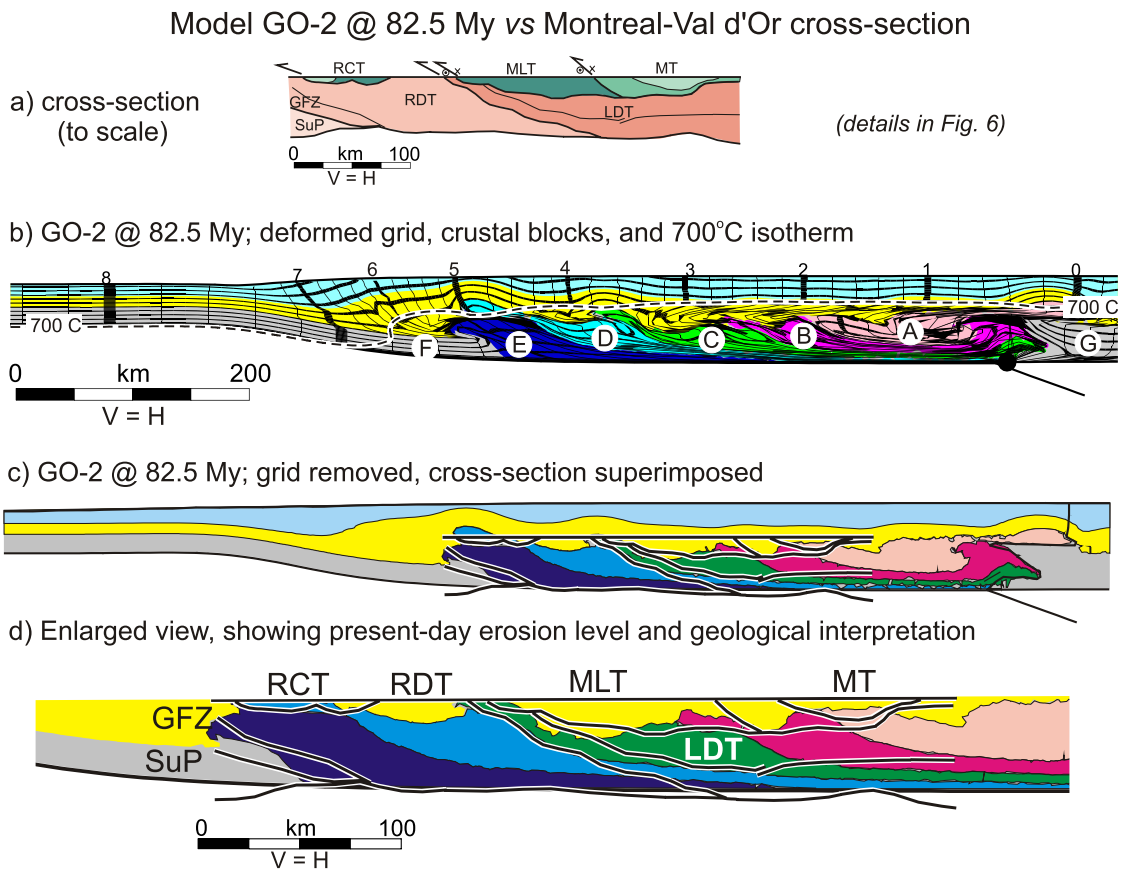

Figure 7. Model GO-2 compared with the Montreal–Val d'Or cross-section. (a) Crustal-scale cross section (Figure 6) at same scale as model. (b) Model result at 82.5 Ma(emt) (My = Ma(emt), showing deformed crustal blocks, marker grid, and 700°C isotherm. Ductile lower crustal nappes (blocks E, D) are stacked against leading edge of lower crustal indentor (F), but total transport distance and amount of exhumation are much less than in model GO-3 (Figure 2, 3, and 5). Orogenic core consists of moderately dipping thrust sheets overlain by weak middle crust that has not been folded into lower crustal ductile flow zone. (c) Model result with marker grid removed for clarity, Montreal–Val d'Or cross section superimposed. (d) Enlarged view of Figure 7c, showing present-day erosion level and geological interpretation. Parautochthon (GFZ, RDT) corresponds to ductile lower crustal blocks D and E, and MLT and MT correspond to melt-weakened middle crust, ductile thrust sheets in infrastructure correspond mainly to LDT. For further discussion, see text.

[34] In contrast to the Georgian Bay transect, the Montreal–Val d'Or transect includes a substantial proportion of reworked Archean rocks (GFZ, RDT) and lacks a significant volume of juvenile rocks formed during Mesoproterozoic arc magmatism. Accreted terranes (RCT, MLT, MT) include a variety of Mesoproterozoic metasedimentary and metaplutonic rocks and anorthosite complexes interpreted as the northern extension of the Frontenac-Adirondack Belt (FAB) [*Carr et al.*, 2000; *Martignole et al.*, 2000]. CAB equivalents are not known from this transect. Allochthonous terranes extend as thin sheets much closer to the GF, and several major structures display oblique or transcurrent kinematics (Figure 6), in some cases overprinting earlier thrusts [e.g., *Martignole*, 1995]. Like the Georgian Bay transect, the entire region south of the GF was affected by Grenvillian upper amphibolite to granulite facies metamorphism and ductile strain. In Laurentian crust (GFZ, RDT, LDT) ages of peak metamorphism and deformation are older in the southeast than the northwest [e.g., *Childe et al.*, 1993; *Friedman and Martignole*, 1995; *Indares and Dunning*, 1997; *Martignole et al.*, 2000]. Accreted terranes (RCT, MLT, MT) record early (circa 1160–1180 Ma) granulite facies metamorphism and deformation not seen in adjacent and underlying rocks and were not strongly overprinted by Ottawan effects.

[35] Figure 7 shows model GO-2 at 82.5 Ma(emt) compared with the Montreal–Val d'Or cross section. At this stage of model evolution, weaker internal blocks (A, B, C, D) have been stacked over stronger external blocks (E, F), with the nose of block D forming a thin detached klippe above block E (Figure 7b). Beneath the plateau, the 700°C isotherm is parallel to the surface and lies near the base of the middle crustal layer; isotherms are steepened and stretched near the orogenic front, but are not overturned.

Figure 7c shows a line drawing of the cross section superimposed on the 82.5 Ma(emt) model result. The cross section and model have been aligned at the Moho, with the leading edge of block F aligned with the leading edge of the Superior craton (SuP), and the boundary between blocks D and C aligned with the base of the LDT. There is a good correspondence between the geometries of the cross section and the model (Figure 7d). The GFZ encompasses the boundary between blocks F and E, consistent with the transition from Archean foreland to parautochthon within this zone. Lower crustal blocks E and D correspond to the interpreted subsurface position of the RDT, and block C largely overlaps with the position of the LDT. The base of the detached block D klippe corresponds to the base of the RCT, and the base of the middle crustal layer broadly coincides with the base of the MLT and MT.

[36] The hallmarks of model GO-2 that best match the Montreal–Val d'Or transect are (1) the position of the leading edge of the Superior craton, which forms a crustal-scale ramp beneath the outer edge of the orogen; (2) the relatively short distance between the GF and the leading edge of allochthonous terranes; (3) thin, flat-lying allochthonous sheets overlying a large volume of reworked (parautochthonous) lower crust; (4) moderately dipping structures in the orogenic infrastructure; and (5) the boundary between ductile middle and lower crust that corresponds roughly to the lower boundary of the FAB terranes. These features are achieved in model GO-2 at about 82.5 Ma(emt), corresponding to the onset of collision with the strong external lower crust. The shorter time, and correspondingly less convergence, compared to model GO-3, may reflect later onset of Ottawan convergence in this region, as suggested by some geochronological data [e.g., *Childe et al.*, 1993; *Indares and Dunning*, 1997; *Carr et al.*, 2000], and/or oblique convergence, as suggested by surface structures (Figure 6) [*Martignole et al.*, 2000]. At this stage of convergence, there has been enough phase 3 activation of the infrastructure that fold nappes have been created and stacked within the orogenic core, but wholesale expulsion over the crustal ramp has only just started. The lower erosion rate in GO-2 versus GO-3 favors lateral transport of thin sheet-like nappes rather than exhumation of thick coherent thrust sheets, compatible with the observed contrasts between the Montreal–Val d'Or and Georgian Bay transects.

[37] However, in this case, the geological correspondence is not as good as it is for the Georgian Bay versus GO-3 comparison, particularly with respect to the pre-Ottawan position of the accreted terranes. Rather than corresponding to outboard blocks A, B, and C, RCT overlaps with the leading edge of block D, and MLT and MT largely overlap with middle crust that originally lay above blocks A to C. This may indicate that at the onset of Ottawan deformation, FAB accreted terranes were already partially exhumed and/or well advanced over the Laurentian margin, so that they occupied the region corresponding to the middle crust in the model. Alternatively, the model lower crust may be too thin. Despite these geological discrepancies, the good geometrical correspondence suggests that the model has captured some of the essential elements of Ottawan convergence along the Montreal–Val d'Or transect.

5. Discussion

5.1. Implications for Grenvillian Tectonics

[38] The good correspondence between GO-model results and crustal-scale cross sections from the western Grenville orogen shows that the variable-strength crust numerical model can make geologically reasonable predictions for orogenic belts that were constructed from laterally heterogeneous crust. The models were designed to investigate how a generic accretionary margin consisting of blocks with different compositions and/or tectonic histories would respond to convergence between bounding cratonic nuclei, driven by simple suborogenic subduction. It was not anticipated that such deliberately simplified initial model structure and tectonic boundary conditions would reproduce observed crustal-scale architecture with some fidelity. While the present models do not account for all aspects of Grenvillian tectonics, the following general interpretation is compatible with both first-order geological constraints and model predictions (Figure 8).

[39] Prior to the Ottawan orogeny, the southeastern margin of Laurentia consisted of the Archean Superior craton flanked by variably reworked Paleoproterozoic to Mesoproterozoic rocks, including a substantial volume of continental magmatic arc and back-arc material. Pre-Ottawan accretionary episodes (Elzevirian and Shawinigan phases [*Rivers and Corrigan*, 2000]) led to the assembly of a variety of accreted terranes at or near the southeastern edge of Laurentia. These included the CAB and associated rocks in the region of the Georgian Bay transect, and the FAB and equivalents in the region of the Montreal–Val d'Or transect. The combination of pre-Grenvillian tectonic history and early Grenvillian accretion produced the lateral crustal strength variations taken as the starting point for the GO model series. The models apply only to the Ottawan-Rigolet stages (circa 1090–990 Ma) and offer no insight into the nature or duration of pre-Ottawan accretionary episodes.

[40] The models are driven by cryptic subduction that dips away from "Laurentia." Since the polarity and dip of suborogenic subduction have relatively little effect on large hot orogen models [*Jamieson et al.*, 2002; *Beaumont et al.*, 2004], the nature of Ottawan subduction is not constrained by the model. However, the assumed subduction polarity is compatible with the recent recognition of a SE dipping, slab-like, high-velocity anomaly in the sublithospheric mantle beneath the western Grenville orogen [*Aktas and Eaton*, 2006]. For simplicity, the initial model crust is symmetric (Figure 1a), and the model "Laurentia" collides with an equivalent opposing margin, with an intervening strong cratonic block. The identity of the continent that collided with Laurentia has not been firmly established, although it is widely thought to have been part of Amazonia [e.g., *Hoffman*, 1991; *Tohver et al.*, 2006]. The GO model series requires only that the colliding continent included lower crustal material that was stronger than the Laurentian margin and its accreted terranes.

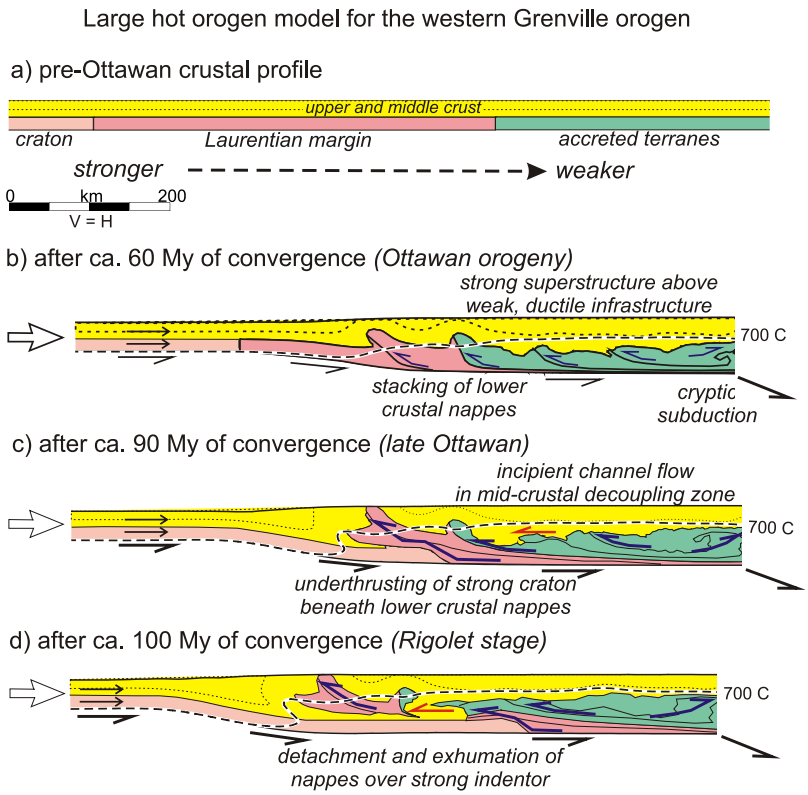

Figure 8. Tectonic interpretation for western Grenville orogen, adapted from model GO-3. Only the crust is shown; underlying mantle is not deformed. Center of orogen is to right of illustrated region. Arrows show tectonic convergence, ductile flow and transport of lower crustal nappes, and incipient channel flow in melt-weakened midcrust (My = Ma(emt)). (a) Prior to the onset of Ottawan convergence, the Superior craton was flanked by progressively weaker Laurentian margin crust and terranes assembled during earlier accretionary episodes. (b) During Ottawan convergence, weaker lower crustal terranes (orogenic core) are deformed against and stacked over adjacent stronger terranes, forming a ductile infrastructure beneath a stonger upper crustal superstructure. (c) Transport of the strong craton beneath the orogen activates lateral flow in the ductile infrastructure, leading to transport and exhumation of ductile nappes over lower crustal indentor. (d) At the end of convergence (Rigolet stage), coherent lower crustal nappes are detached from their roots, transported over the indentor, and rapidly exhumed.

[41] In the models, deformation propagates from the model suture (marker 0, boundary between blocks A and G) toward the craton (block F). Upper and middle crustal layers are shortened but retain upright structures, except for the lowermost middle crust, which is affected by the high temperatures and pervasive ductile flow that characterize the internal lower crustal blocks (A to D). Transport of the detached nose of block C in the midcrustal flow zone explains the observed position of the PSD klippe, and suggests that other lower crustal fragments, including relict high-pressure rocks [e.g., *Ketchum and Davidson*, 2000], may have undergone similar amounts and styles of displacement [cf. *Jamieson et al.*, 2004, Figure 11]. These model predictions are compatible with the observations that ages of Ottawan deformation and metamorphism generally young from southeast to northwest [e.g., *Jamieson et al.*, 1992; *Culshaw et al.*, 1997], and that pre-Ottawan ages are preserved at high structural levels [*Carr et al.*, 2000; *Martignole et al.*, 2000]. In the western Grenville orogen, this implies that the exposed parts of the PSD, CAB, RCT, MLT, and MT were in the midcrust prior to the onset of the Ottawan orogeny, consistent with previous interpretations [e.g., *Culshaw et al.*, 1997; *Carr et al.*, 2000; *Martignole et al.*, 2000; *Wodicka et al.*, 2000].

[42] In model GO-3, melt-weakened middle crust is drawn into the ductile flow region, where it is infolded with lower crustal nappes and affected by incipient channel flow. Moderate erosion enhances lateral transport and partial exhumation of the leading edges of blocks B, C, and D, detaching them from their lower crustal roots and allowing melt-weakened midcrust to flow into the gaps. Along the Georgian Bay transect, the highly migmatitic Shawanaga domain and Seguin and Moon River lobes of the Muskoka domain (Figure 4), which lie beneath and above the Parry Sound domain klippe respectively [e.g., *Culshaw et al.*, 1994, 1997; *Slagstad et al.*, 2005], may correspond to this melt-weakened midcrustal material. The Montreal–Val d'Or transect and corresponding model GO-2 lack this type of feature (Figures 6 and 7).

[43] In the models, collision with strong lower crustal blocks E and F, which resist ductile deformation, leads to a marked change in tectonic style. Lateral ductile flow beneath the decoupling zone, characteristic of weaker crust in the interior of the orogen, is replaced by transport and partial exhumation of nappes over the ramp formed by the leading edge of indentor block F. In nature, this transition may have coincided with the arrival of Archean crust beneath the flank of the orogen, and may account for the contrast in tectonic style between the Grenville Front Tectonic Zone and adjacent parautochthon relative to more internal parts of the orogen. Work in progress will address late orogenic extensional features, which are not accounted for in the present models.

[44] The GO series models presented here, while accounting for the crustal-scale architecture of the western part of the orogen, cannot be considered realistic for the orogen as a whole. For example, these models do not predict exhumation of the coherent high-pressure terranes observed in eastern Quebec and Labrador [e.g., *Rivers et al.*, 2002]. This has been interpreted to reflect significant along-strike differences in pre-Grenvillian crustal properties [e.g., *Warren et al.*,. 2006], beyond the range considered in the present study.

5.2. Implications for Ductile Flow in Large Hot Orogens

[45] One goal of the present study was to determine how the style of lower crustal flow in large hot orogens with laterally variable strength differs from that displayed by orogens constructed from laterally homogeneous crust. Model results show clear contrasts between the crustal structure and tectonic evolution of the GO series models and that of HT-style homogeneous channel flow models (Figure 9) [*Beaumont et al.*, 2001, 2004, 2006; *Jamieson et al.*, 2004]. In channel flow models, laterally homogeneous crust evolves to become sufficiently hot and weak that the midcrustal infrastructure flows laterally as a channel under gravitational forces alone (Figure 9a). The driving forces result from the lateral pressure difference between the foreland and thickened crust underlying the orogenic plateau [e.g., *Bird*, 1991; *Clark and Royden*, 2000; *Hodges et al.*, 2001; *Hodges*, 2006], and low midcrustal viscosities ($\eta_{eff} \leq 10^{19}$ Pa s) are required for significant channel flows to develop [*Royden*, 1996; *Beaumont et al.*, 2001]. In contrast, GO series models can activate and expel relatively high viscosity midcrustal and lower crustal nappes from the orogen interior because the force driving the indentation is tectonic; the process is probably limited only by the strength of the indentor (Figure 9b). Although the midcrustal regions of GO-type models are melt weakened and display incipient channel flow, this behavior is subordinate to the creation and expulsion of ductile lower crustal nappes. However, like the channel flow models, the GO model system is constrained by the weight of the plateau crust, so that the height and tilt of the plateau monitor ambient pressure and tractions within the orogen. Natural equivalents of GO-type models must therefore operate with plateau conditions that accord with observations, currently limited to elevations of $\sim$5.5 km.

[46] Observations and model predictions [e.g., *Godin et al.*, 2006; *Beaumont et al.*, 2006] suggest that channel flow and other ductile flow modes share a number of features, including large-scale lateral transport, association with orogenic plateaus, diachronous evolution with deformation propagating from the orogenic core toward the foreland, and pervasive ductile deformation and transposition. Distinctive features of homogeneous channel flow in natural orogens include (Figure 9a) (1) a significant volume of low-viscosity material (10–20 km thick) between underlying and overlying higher viscosity rocks; (2) pervasive melt-present deformation, with leucosomes younger than shortening structures in crust overlying the channel; (3) demonstrably coeval shear zones with thrust and normal fault geometries at the lower and upper boundaries of the channel flow zone, and kinematic inversion from thrust to normal sense shear along the roof shear zone; (4) inverted and right way-up metamorphic sequences at the base and top of the extruding channel; and (5) lack of continuity between preexisting structures above, within, and below the channel [*Godin et al.*, 2006]. Where these features cannot be reliably identified, the GO series models provide an alternative mechanism for large-scale lateral ductile flow during convergence. Distinctive characteristics of this flow style include (Figure 9b) (1) assembly and stacking of coherent ductile thrust sheets and/or nappes; (2) transport of detached lower crustal fragments in the ductile flow zone; (3) a link between inferred precollision strength and stacking order, with weaker materials systematically thrust over stronger materials; and (4) the inferred or demonstrated presence of a strong lower crustal indentor.

[47] A particular characteristic of Grenville-style orogens that can be addressed by generic GO series models is the degree of allochthoneity of lower crust, which in the models is expressed by the relative uplift and lateral expulsion of lower crust from the interior of the orogen toward the foreland. Although in nature this cannot be uniquely attributed to collision with a strong external block, collision with an indentor that underthrusts the hot, weak orogenic core provides a very effective mechanism for creating highly allochthonous lower crustal terranes. In the absence of such a collision, model lower crust would continue to evolve as in phases 1 and 2 of the GO models (Figures 2a–2c), and weak, ductile infrastructure would remain buried in the lower crust rather than being transported up and over the indentor as detached nappes and/or coherent allochthonous thrust sheets (phase 3 flow).

[48] There has been considerable recent speculation on the possible role of channel flow in many large hot orogens. For example, it has been proposed that some form of channel flow affected both the Paleoproterozoic Trans-Hudson orogen [*St-Onge et al.*, 2006] and parts of the Paleozoic Appalachian-Caledonide orogen [*Gilotti and McClelland*, 2005; *Hatcher and Merschat*, 2006]. In the latter case, inferred orogen-parallel channel flow in the southern Appalachian Piedmont has been attributed to 3-D variations in crustal strength [*Hatcher and Merschat*, 2006]. In the southeastern Canadian Cordillera, where a Mesozoic accretionary orogen was constructed at a laterally extensive

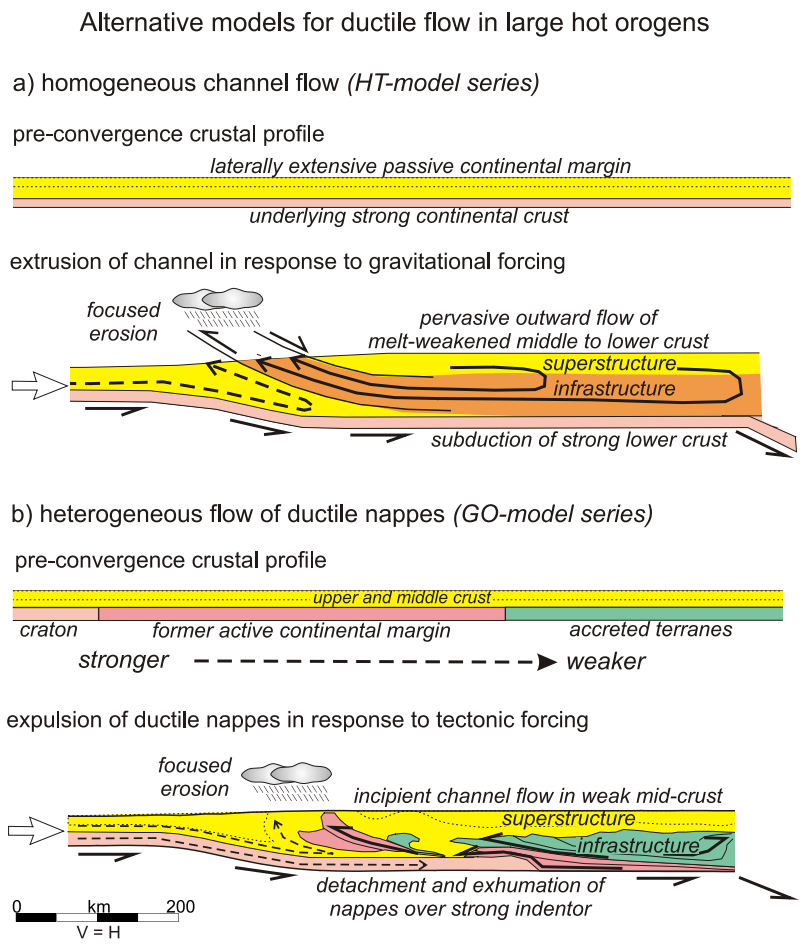

Figure 9. Contrasting ductile flow modes in large hot orogens. Only the crustal domain is shown; underlying mantle is not deformed. Center of orogen is to right of illustrated region. (top) Preconvergence crustal profiles; (bottom) crustal structure at orogenic peak. Arrows show material flow paths. (a) Homogeneous channel flow in Himalayan-style orogens, adapted from HT model series [*Beaumont et al.*, 2004, 2006; *Jamieson et al.*, 2004]. Preorogenic crust consists of laterally extensive passive margin overlying thin, strong lower crust that is subducted during convergence. At the orogenic peak, a 10–20 km thick melt-weakened channel (infrastructure) flows laterally from beneath the plateau (superstructure), driven by the gravitational potential gradient between the plateau and the foreland. Channel is extruded between coeval thrust sense and normal sense shear zones in response to focused erosion at the orogenic front. (b) Heterogeneous flow of ductile nappes in Grenville-style orogens, adapted from GO model series (this work). Preorogenic crust consists of a strong craton flanked by systematically weaker terranes. At the orogenic peak, orogenic core consists of ductile, moderately dipping nappes overlain by incipient (<5 km) channel (infrastructure), with upright structures preserved in upper crust (superstructure). Lateral flow driven by tectonic convergence as outboard lower crustal blocks are transported, detached, and exhumed over strong lower crustal indentor; bounding shear zones at orogenic flank are thrust sense.

continental margin, the applicability of the homogeneous channel flow model is currently under debate [e.g., *Brown and Gibson*, 2006; *Carr and Simony*, 2006]. In modern systems, the channel flow hypothesis has been invoked for the southern flank of the Himalayan-Tibetan system [e.g., *Beaumont et al.*, 2001; *Hodges*, 2006] and the Altiplano-Puna region of the convergent Andean margin [e.g., *Husson and Sempere*, 2003]. In the Himalayan-Tibetan orogen, however, the style of lower crustal flow on the northern side of the system, constructed from the former accretionary margin of south Asia, is not known, and the relatively recent transport of cratonic India beneath the Himalaya could now be inducing a change in tectonic style toward something like that displayed by the GO series models. In short, the applicability of a given model to a particular natural example requires a balanced assessment of all the available evidence, and a recognition that different ductile flow modes, including some not discussed here, may operate at

different stages in the evolution of any large orogenic system [*Beaumont et al.*, 2006].

6. Conclusions

[49] 1. Models with laterally variable lower crustal strength evolve to produce a series of lower crustal nappes, with weaker blocks systematically thrust over adjacent stronger blocks, and eventually detached and expelled as ductile nappes over a lower crustal indentor. Although incipient midcrustal channel flow develops beneath the plateau, the GO models do not display homogeneous Himalayan-type channel flow and associated extrusion.

[50] 2. Model evolution can be described in terms of crustal thickening (phase 1), thermal relaxation (phase 2), and tectonic activation of ductile flow (phase 3) resulting in a ductile orogenic infrastructure underlying a strong superstructure. This evolution is diachronous, affecting internal parts of the model orogen first and propagating toward the foreland with time.

[51] 3. The extent to which lower crust is expelled and exhumed as coherent ductile thrust sheets, is dismembered and transported during pervasive ductile flow, or remains in the midcrust as flattened nappes depends on total convergence and erosion rate at the plateau flank.

[52] 4. Model GO-3 corresponds well to the geometry of the Georgian Bay transect, and GO-2 corresponds well to the Montreal–Val d'Or transect. To a first approximation, this suggests that the Ottawan orogeny involved activation of heterogeneous pre-Ottawan Laurentian crust and accreted terranes as a series of ductile nappes that were progressively stacked, transported, and expelled above strong Archean lower crust. Geometrical contrasts between the two transects in the vicinity of the Grenville Front can be explained in terms of contrasting erosion rate and extent of Archean underthrusting.

[53] 5. The similarity of GO model geometries to the crustal-scale architecture of the western Grenville orogen suggests that this model style is a plausible, albeit highly simplified, representation of a Grenville-style orogen with variable precollision lower crustal strength.

[54] 6. The present results contrast with those of homogeneous channel flow models, and suggest some criteria for distinguishing between ductile flow modes in large hot orogens.

[55] **Acknowledgments.** This work was funded by NSERC Discovery grants to Jamieson, Beaumont, and Culshaw. Regional mapping in the Georgian Bay area was originally funded by an OGS-GSC contract to Culshaw and Lithoprobe Supporting Geoscience grants to Culshaw and Jamieson. Beaumont acknowledges support from the Canada Research Chairs program and an IBM Shared University Research grant. Models were run using computer software developed by P. Fullsack at Dalhousie University. The manuscript benefited from constructive and thorough reviews by T. Rivers and an anonymous referee and helpful comments by T. Ehlers.

References

Aktas, K., and D. W. Eaton (2006), Upper-mantle velocity structure of the lower Great Lakes region, *Tectonophysics*, *420*, 267–281.

Beaumont, C., R. A. Jamieson, M. H. Nguyen, and B. Lee (2001), Himalayan tectonics explained by extrusion of a low-viscosity channel coupled to focused surface denudation, *Nature*, *414*, 738–742.

Beaumont, C., R. A. Jamieson, M. H. Nguyen, and S. Medvedev (2004), Crustal channel flows: 1. Numerical models with applications to the tectonics of the Himalayan-Tibetan orogen, *J. Geophys. Res.*, *109*, B06406, doi:10.1029/2003JB002809.

Beaumont, C., M. H. Nguyen, R. A. Jamieson, and S. Ellis (2006), Crustal flow modes in large hot orogens, in *Channel Flow, Ductile Extrusion, and Exhumation of Lower-Midcrust in Continental Collision Zones*, edited by R. D. Law, M. P. Searle, and L. Godin, *Geol. Soc. Spec. Publ.*, *268*, 91–145.

Bethune, K. M. (1997), The Sudbury dyke swarm and its bearing on the tectonic development of the Grenville Front, Ontario, Canada, *Precambrian Res.*, *85*, 117–146.

Bird, P. (1991), Lateral extrusion of lower crust from under high topography, in the isostatic limit, *J. Geophys. Res.*, *96*, 10,275–10,286.

Bridgwater, D., V. R. McGregor, and J. S. Myers (1974), A horizontal tectonic regime in the Archean of Greenland and its implications for early crustal thickening, *Precambrian Res.*, *1*, 179–197.

Brown, R., and H. D. Gibson (2006), An argument for channel flow in the southern Canadian Cordillera and comparison with Himalayan tectonics, in *Channel Flow, Ductile Extrusion, and Exhumation of Lower-Midcrust in Continental Collision Zones*, edited by R. D. Law, M. P. Searle, and L. Godin, *Geol. Soc. Spec. Publ.*, *268*, 543–559.

Burr, J. L., and S. D. Carr (1994), Structural geometry and U-Pb geochronology near Lithoprobe seismic line 32, western Central Metasedimentary Belt, Grenville Province, Ontario: New results from high precision U-Pb geochronology, paper presented at Abitibi-Grenville Transect Workshop, Univ. of Montreal, Montreal, Que., Canada, 14–15 April.

Card, K. D. (1990), A review of the Superior Province of the Canadian Shield: A product of Archean accretion, *Precambrian Res.*, *48*, 99–156.

Carlson, K. A., B. A. van der Pluijm, and S. Hanmer (1990), Marble mylonites of the Bancroft shear zone: Evidence for extension in the Canadian Grenville, *Geol. Soc. Am. Bull.*, *102*, 174–181.

Carr, S. D., and P. S. Simony (2006), Ductile thrusting versus channel flow in the southeastern Canadian Cordillera: Evolution of a coherent crystalline thrust sheet, in *Channel flow, Ductile Extrusion, and Exhumation of Lower-Midcrust in Continental Collision Zones*, edited by R. D. Law, M. P. Searle, and L. Godin, *Geol. Soc. Spec. Publ.*, *268*, 561–587.

Carr, S. D., R. M. Easton, R. A. Jamieson, and N. G. Culshaw (2000), Geologic transect across the Grenville orogen of Ontario and New York, *Can. J. Earth Sci.*, *37*, 193–216.

Childe, F., R. Doig, and C. Gariépy (1993), Monazite as a metamorphic chronometer, south of the Grenville Front, western Quebec, *Can. J. Earth Sci.*, *30*, 1056–1065.

Clark, M. K., and L. H. Royden (2000), Topographic ooze: Building the eastern margin of Tibet by lower crustal flow, *Geology*, *28*, 703–706.

Corfu, F., and R. M. Easton (1995), U-Pb geochronology of the Mazinaw terrane, an imbricate segment of the Central Metasedimentary Belt, Grenville Province, Ontario, *Can. J. Earth Sci.*, *32*, 959–976.

Corfu, F., and R. M. Easton (1997), Sharbot Lake terrane and its relationships to Frontenac terrane, Central Metasedimentary Belt, Grenville Province: New insights from U-Pb geochronology, *Can. J. Earth Sci.*, *34*, 1239–1257.

Corrigan, D., N. G. Culshaw, and J. K. Mortensen (1994), Pre-Grenvillian evolution and Grenvillian overprinting of the Parautochthonous Belt in the Key Harbour area, Ontario; U-Pb constraints, *Can. J. Earth Sci.*, *31*, 160–175.

Corriveau, L., and O. van Breemen (2000), Docking of the Central Metasedimentary Belt to Laurentia in geon 12: Evidence from the 1.17–1.16 Ga Chevreuil intrusive suite and host gneisses, Quebec, *Can. J. Earth Sci.*, *37*, 253–269.

Culshaw, N., and J. Dostal (1997), Sand Bay gneiss association, Grenville Province, Ontario: A Grenvillian rift (and -drift) assemblage strained in the Central Gneiss Belt, *Precambrian Res.*, *85*, 97–113.

Culshaw, N. G., J. W. F. Ketchum, N. Wodicka, and P. I. Wallace (1994), Ductile extension following thrusting in the deep crust: Evidence from the southern Britt Domain, southwest Grenville Province, Georgian Bay, Ontario, *Can. J. Earth Sci.*, *31*, 160–175.

Culshaw, N. G., R. A. Jamieson, J. W. F. Ketchum, N. Wodicka, D. Corrigan, and P. H. Reynolds (1997), Transect across the northwestern Grenville orogen, Georgian Bay, Ontario: Polystage convergence and extension in the lower orogenic crust, *Tectonics*, *16*, 966–982.

Culshaw, N. G., C. Beaumont, and R. A. Jamieson (2004), Geodynamic models of contrasting structural styles and ages in upper- and lower-crust of collisional orogens: Resolution of the structural vs seismic paradox, *Geol. Assoc. Can. Abstr.*, *29*, 331.

Culshaw, N. G., C. Beaumont, and R. A. Jamieson (2006), The orogenic superstructure-infrastructure concept revisited, quantified, and revived, *Geology*, *34*, 733–736.

Davidson, A. (1984), Tectonic boundaries within the Grenville Province of the Canadian Shield, *J. Geodyn.*, *1*, 433–444.

Davidson, A. (1986a), A new look at the Grenville Front in Ontario, in *Ottawa '86, Field Trip Guidebook 15*, Geol. Assoc. of Can.–Mineral. Assoc. of Can., St. John's, Newfoundland.

Davidson, A. (1986b), New interpretations in the southwestern Grenville province, in *The Grenville Province*, edited by J. M. Moore, A. Davidson, and A. J. Baer, *Spec. Pap. Geol. Assoc. Can.*, *31*, 61–74.

Davidson, A. (1992), Relationship between faults in the Southern Province and the Grenville Front southeast of Sudbury, Ontario, in Current Research, Part C, *Geol. Surv. Can. Pap.*, *92-1C*, 121–127.

Davidson, A. (1995), A review of the Grenville orogen in its North American type area, *J. Aust. Geol. Geophys.*, *16*, 3–24.

Davidson, C., S. M. Schmid, and L. S. Hollister (1994), Role of melt during deformation in the deep crust, *Terra Nova*, *6*, 133–142.

Dickin, A. P., and R. H. McNutt (1991), Nd model-age mapping of Grenville lithotectonic domains: Mid-Proterozoic crustal evolution in Ontario, in *Mid-Proterozoic Laurentia-Baltica*, edited by C. F. Gower, T. Rivers, and B. Ryan, *Spec. Pap. Geol. Assoc. Can.*, *38*, 79–94.

Doig, R. (1991), U-Pb zircon dates of Morin anorthosite suite rocks, Grenville Province, Quebec, *J. Geol.*, *99*, 729–738.

Easton, R. M. (1992), The Grenville Province and the Proterozoic history of central and southern Ontario, in *Geology of Ontario*, *Spec. Vol. 4*, edited by P. C. Thurston et al., pp. 715–904, Ont. Geol. Surv., Sudbury.

Friedman, R., and J. Martignole (1995), Mesoproterozoic sedimentation, magmatism, and metamorphism in the southern part of the Grenville Province (western Quebec): U-Pb geochronological constraints, *Can. J. Earth Sci.*, *32*, 2103–2114.

Fullsack, P. (1995), An arbitrary Lagrangian-Eulerian formulation for creeping flows and its application in tectonic models, *Geophys. J. Int.*, *120*, 1–23.

Gilotti, J. A., and W. C. McClelland (2005), Leucogranites and the time of extension in the East Greenland Caledonides, *J. Geol.*, *115*, 399–417.

Gleason, G. C., and J. Tullis (1995), A flow law for dislocation creep of quartz aggregates determined with the molten salt cell, *Tectonophysics*, *247*, 1–23.

Godin, L., D. Grujic, R. D. Law, and M. P. Searle (2006), Channel flow, ductile extrusion, and exhumation in continental collision zones: An introduction, in *Channel Flow, Ductile Extrusion, and Exhumation of Lower-Midcrust in Continental Collision Zones*, edited by R. D. Law, M. P. Searle, and L. Godin, *Geol. Soc. Spec. Publ.*, *268*, 1–23.

Green, A. G., B. Milkereit, A. Davidson, C. Spencer, D. R. Hutchinson, W. F. Cannon, M. W. Lee, W. F. Agena, J. C. Behrendt, and W. J. Hinze (1988), Crustal structure of the Grenville Front and adjacent terranes, *Geology*, *16*, 788–792.

Grujic, D., M. Casey, C. Davidson, L. S. Hollister, R. Kundig, T. Pavlis, and S. Schmid (1996), Ductile extrusion of the Higher Himalayan Crystalline in Bhutan: Evidence from quartz microfabrics, *Tectonophysics*, *260*, 21–43.

Haggart, M. J., R. A. Jamieson, P. H. Reynolds, T. E. Krogh, C. Beaumont, and N. G. Culshaw (1993), Last gasp of the Grenville orogeny—Thermochronology of the Grenville Front Tectonic Zone near Killarney, Ontario, *J. Geol.*, *101*, 575–589.

Hanmer, S., and S. J. McEachern (1992), Kinematical and rheological evolution of a crustal-scale ductile thrust zone, Central Metasedimentary Belt, Grenville orogen, Ontario, *Can. J. Earth Sci.*, *29*, 1779–1790.

Harris, L. B., B. Rivard, and L. Corriveau (2001), Structure of the Lac Nominingue–Mont Laurier region, Central Metasedimentary Belt, Quebec Grenville Province, *Can. J. Earth Sci.*, *38*, 787–802.

Hatcher, R. D., and A. J. Merschat (2006), The Appalachian Inner Piedmont: An exhumed strike-parallel, tectonically forced orogenic channel, in *Channel Flow, Ductile Extrusion, and Exhumation of Lower-Midcrust in Continental Collision Zones*, edited by R. D. Law, M. P. Searle, and L. Godin, *Geol. Soc. Spec. Publ.*, *268*, 517–541.

Hoffman, P. F. (1991), Did the breakup of Laurentia turn Gondwanaland inside out?, *Science*, *252*, 1409–1411.

Hodges, K. V. (2006), A synthesis of the channel flow–extrusion hypothesis as developed for the Himalayan-Tibetan orogenic system, in *Channel Flow, Ductile Extrusion, and Exhumation of Lower-Midcrust in Continental Collision Zones*, edited by R. D. Law, M. P. Searle, and L. Godin, *Geol. Soc. Spec. Publ.*, *268*, 71–90.

Hodges, K. V., J. M. Hurtado, and K. X. Whipple (2001), Southward extrusion of Tibetan crust and its effect on Himalayan tectonics, *Tectonics*, *20*, 799–809.

Husson, L., and T. Sempere (2003), Thickening the Altiplano crust by gravity-driven crustal channel flow, *Geophys. Res. Lett.*, *30*(5), 1243, doi:10.1029/2002GL016877.

Indares, A., and G. R. Dunning (1997), Coronitic metagabbro and eclogite from the Grenville Province of western Quebec: Interpretation of U-Pb geochronology and metamorphism, *Canadian J. Earth Sci.*, *34*, 891–901.

Indares, A., and J. Martignole (1989), The Grenville Front south of Val d'Or, *Tectonophysics*, *157*, 221–239.

Indares, A., and J. Martignole (1990a), Metamorphic constraints on the evolution of the gneisses from the parautochthonous and allochthonous polycyclic belts, Grenville Province, western Quebec, *Can. J. Earth Sci.*, *27*, 357–370.

Indares, A., and J. Martignole (1990b), Metamorphic constraints on the evolution of the gneisses of the allochthonous monocyclic belt, Grenville Province, western Quebec, *Can. J. Earth Sci.*, *27*, 371–386.

Jamieson, R. A., N. G. Culshaw, N. Wodicka, D. Corrigan, and J. W. F. Ketchum (1992), Timing and tectonic setting of Grenvillian metamorphism—Constraints from a transect along Georgian Bay, Ontario, *J. Metamorph. Geol.*, *10*, 321–332.

Jamieson, R. A., N. G. Culshaw, and D. Corrigan (1995), North-west propagation of the Grenville orogen: Grenvillian structure and metamorphism near Key Harbour, Georgian Bay, Ontario, Canada, *J. Metamorph. Geol.*, *13*, 185–207.

Jamieson, R. A., C. Beaumont, M. H. Nguyen, and B. Lee (2002), Interaction of metamorphism, deformation, and exhumation in large convergent orogens, *J. Metamorph. Geol.*, *20*, 9–24.

Jamieson, R. A., C. Beaumont, S. Medvedev, and M. H. Nguyen (2004), Crustal channel flows: 2. Numerical models with implications for metamorphism in the Himalayan-Tibetan orogen, *J. Geophys. Res.*, *109*, B06407, doi:10.1029/2003JB002811.

Jamieson, R. A., C. Beaumont, M. H. Nguyen, N. G. Culshaw, and T. Slagstad (2005), Melt-weakening and flow modes in large hot orogens: Numerical models with application to the western Grenville orogen, *Geol. Assoc. Can. Abstr.*, *30*, 96.

Ketchum, J. W. F., and A. Davidson (2000), Crustal architecture and tectonic assembly of the Central Gneiss Belt, southwestern Grenville Province, Canada: A new interpretation, *Canadian J. Earth Sci.*, *37*, 217–234.

Ketchum, J. W. F., R. A. Jamieson, L. M. Heaman, N. G. Culshaw, and T. E. Krogh (1994), 1.45 Ga granulites in the southwestern Grenville Province: Geologic setting, *P-T* conditions, and U-Pb geochronology, *Geology*, *22*, 215–218.

Ketchum, J. W. F., L. M. Heaman, T. E. Krogh, N. G. Culshaw, and R. A. Jamieson (1998), Timing and thermal influence of late orogenic extension in the lower crust: A U-Pb geochronological study from the southwest Grenville orogen, Canada, *Precambrian Res.*, *89*, 25–45.

Koons, P. O. (1989), The topographic evolution of collisional mountain belts: A numerical look at the Southern Alps, New Zealand, *Am. J. Sci.*, *289*, 1041–1069.

Krogh, T. E. (1994), Precise U-Pb ages for Grenvillian and pre-Grenvillian thrusting of Proterozoic and Archean metamorphic assemblages in the Grenville Front Tectonic Zone, Canada, *Tectonics*, *13*, 963–982.

Krogh, T. E., and Y. Y. Kwok (2005), The age enigma in the Moon River structure and the Parry Sound domain connection, Grenville Province, *Geol. Assoc. Can. Abstr.*, *30*, 106.

Mackwell, S. J., M. E. Zimmerman, and D. L. Kohlstedt (1998), High-temperature deformation of dry diabase with application to tectonics on Venus, *J. Geophys. Res.*, *103*, 975–984.

Martignole, J. (1995), Reply: A two-stage emplacement for the Cabonga allochthon (central part of the Grenville Province): Evidence for orthogonal and oblique collision during the Grenville orogeny, *Can. J. Earth Sci.*, *32*, 1478–1481.

Martignole, J., and A. J. Calvert (1996), Crustal-scale shortening and extension across the Grenville Province of western Quebec, *Tectonics*, *15*, 376–386.

Martignole, J., and R. Friedman (1998), Geochronological constraints on the last stages of terrane assembly in the central part of the Grenville Province (Quebec), *Precambrian Res.*, *92*, 145–164.

Martignole, J., and P. H. Reynolds (1997), $^{40}Ar/^{39}Ar$ thermochronology along a western Quebec transect of the Grenville Province, Canada, *J. Metamorph. Geol.*, *15*, 283–296.

Martignole, J., A. J. Calvert, R. Friedman, and P. H. Reynolds (2000), Crustal evolution along a seismic section across the Grenville Province (western Quebec), *Can. J. Earth Sci.*, *27*, 291–306.

Myers, J. S. (1978), Formation of banded gneisses by deformation of igneous rocks, *Precambrian Res.*, *6*, 43–64.

Nadeau, L., and O. van Breemen (1998), Plutonic ages and tectonic setting of the Algonquin and Muskoka allochthons, Central Gneiss Belt, Grenville Province, Ontario, *Can. J. Earth Sci.*, *35*, 1423–1438.

Northrup, C. J. (1996), Structural expression and tectonic implications of general noncoaxial flow in the midcrust of a collisional orogen: The northern Scandinavian Caledonides, *Tectonics*, *15*, 490–505.

Rivers, T. (1997), Lithotectonic elements of the Grenville Province: Review and tectonic implications, *Precambrian Res.*, *86*, 117–154.

Rivers, T., and D. Corrigan (2000), Convergent margin on southeastern Laurentia during the Mesoproterozoic: Tectonic implications, *Can. J. Earth Sci.*, *37*, 359–383.

Rivers, T., J. Martignole, C. F. Gower, and A. Davidson (1989), New tectonic divisions of the Grenville Province, southeast Canadian Shield, *Tectonics*, *8*, 63–84.

Rivers, T., J. W. F. Ketchum, A. Indares, and A. Hynes (2002), The high pressure belt in the Grenville Province: Architecture, timing and exhumation, *Can. J. Earth Sci.*, *39*, 867–893.

Rivers, T., N. Culshaw, A. Hynes, A. Indares, R. A. Jamieson, and J. Martignole (2006), The Grenville Orogen, in *Variations in Tectonic Styles Revisited: A Lithoprobe Perspective*, edited by J. Percival, *Spec. Pap. Geol. Assoc. Can.*, submitted.

Rosenberg, C. L., and M. R. Handy (2005), Experimental deformation of partially melted granite revisited: Implications for the continental crust, *J. Metamorph. Geol.*, *23*, 19–28.

Royden, L. H. (1996), Coupling and decoupling of crust and mantle in convergent orogens: Implications for strain partitioning in the crust, *J. Geophys. Res.*, *101*, 17,679–17,705.

Slagstad, T., N. G. Culshaw, R. A. Jamieson, and J. W. F. Ketchum (2004a), Early Proterozoic tectonic history of the southwestern Grenville Province, Ontario: Constraints from geochemistry and geochronology of high-grade gneisses, in *Proterozoic Tectonic Evolution of the Grenville Orogen in North America*, edited by R. P. Tollo et al., *Mem. Geol. Soc. Am.*, *197*, 209–241.

Slagstad, T., M. A. Hamilton, R. A. Jamieson, and N. G. Culshaw (2004b), Timing and duration of melting

in the mid-orogenic crust: Constraints from U-Pb (SHRIMP) data, Muskoka and Shawanaga domains, Grenville Province, Ontario, *Can. J. Earth Sci.*, *41*, 1339–1365.

Slagstad, T., R. A. Jamieson, and N. G. Culshaw (2005), Formation, crystallisation, and migration of melt in the mid-orogenic crust: Muskoka domain migmatites, Grenville Province, Ontario, *J. Petrol.*, *46*, 893–919.

St-Onge, M. R., M. P. Searle, and N. Wodicka (2006), The Trans-Hudson orogen of North America and the Himalaya-Karakoram-Tibetan orogen of Asia: Structural and thermal characteristics of the lower and upper plates, *Tectonics*, *25*, TC4006, doi:10.1029/2005TC001907.

Timmermann, H., R. R. Parrish, R. A. Jamieson, and N. G. Culshaw (1997), Time of metamorphism beneath the Central Metasedimentary Belt Boundary Thrust Zone, Grenville Orogen, Ontario: Accretion at 1080 Ma?, *Can. J. Earth Sci.*, *34*, 1023–1029.

Tohver, E., W. Teixeira, B. van der Pluijm, M. C. Geraldes, J. S. Bettencourt, and G. Rizzotto (2006), Restored transect across the exhumed Grenville orogen of Laurentia and Amazonia, with implications for crustal architecture, *Geology*, *34*, 669–672.

Tollo, R. P., L. Corriveau, J. McLelland, and M. J. Bartholemew (2004), Proterozoic evolution of the Grenville orogen in North America: An introduction, in *Proterozoic Tectonic Evolution of the Grenville Orogen in North America*, edited by R. P. Tollo et al., *Mem. Geol. Soc. Am.*, *197*, 1–18.

van Breemen, O., A. Davidson, W. D. Loveridge, and R. D. Sullivan (1986), U-Pb zircon geochronology of Grenvillian tectonites, granulites and igneous precursors, Parry Sound, Ontario, in *The Grenville Province*, edited by J. M. Moore, A. Davidson, and A. J. Baer, *Spec. Pap. Geol. Assoc. Can.*, *31*, 191–207.

Warren, C. J., R. A. Jamieson, C. Beaumont, and M. H. Nguyen (2006), Does east meet west? Insights into the thermal-tectonic evolution of the Central Gneiss Belt and Manicouagan Imbricate Zone from numerical modeling, *Geol. Assoc. Can. Abstr.*, *31*, 160.

Westaway, R. (1995), Crustal volume balance during the India-Eurasia collision and altitude of the Tibetan Plateau: A working hypothesis, *J. Geophys. Res.*, *100*, 15,173–15,192.

White, D. J., R. M. Easton, N. G. Culshaw, B. Milkereit, D. A. Forsyth, S. D. Carr, A. G. Green, and A. Davidson (1994), Seismic images of the Grenville Orogen in Ontario, *Can. J. Earth Sci.*, *31*, 293–307.

White, D. J., D. A. Forsyth, I. A. Asudeh, S. D. Carr, H. Wu, R. M. Easton, and R. F. Mereu (2000), Seismic-based cross-section across the Grenville Front in Ontario, *Can. J. Earth Sci.*, *37*, 183–192.

Willett, S. D. (1999), Orogeny and orography: The effects of erosion on the structure of mountain belts, *J. Geophys. Res.*, *104*, 28,957–28,981.

Williams, M. L., and S. Hanmer (2006), Structural and metamorphic processes in the lower crust: Evidence from the East Athabasca mylonite triangle, Canada: A deep-crustal isobarically cooled terrane, in *Evolution and Differentiation of the Continental Crust*, edited by M. Brown and T. Rushmer, pp. 231–267, Cambridge Univ. Press, Cambridge, U. K.

Wodicka, N., R. R. Parrish, and R. A. Jamieson (1996), The Parry Sound domain: A far-travelled allochthon? New evidence from U-Pb zircon geochronology, *Can. J. Earth Sci.*, *33*, 1087–1104.

Wodicka, N., J. W. F. Ketchum, and R. A. Jamieson (2000), Grenvillian metamorphism of monocyclic rocks, Georgian Bay, Ontario, Canada: Implications for convergence history, *Can. Mineral.*, *38*, 471–510.

Wynne-Edwards, H. R. (1972), The Grenville Province, in *Variations in Tectonic Styles in Canada*, edited by R. A. Price and R. J. W. Douglas, *Spec. Pap. Geol. Assoc. Can.*, *11*, 263–334.

Zeitler, P. K., et al. (2001), Crustal reworking at Nanga Parbat, Pakistan: Metamorphic consequences of thermal-mechanical coupling facilitated by erosion, *Tectonics*, *20*, 712–728.

C. Beaumont, Department of Oceanography, Dalhousie University, Halifax, NS, Canada B3H 4J1.

N. G. Culshaw, R. A. Jamieson, and M. H. Nguyen, Department of Earth Sciences, Dalhousie University, Halifax, NS, Canada B3H 3J5. (beckyj@dal.ca)